Aerosol Effects on Electrification and Lightning Discharges in a Multicell Thunderstorm Simulated by the WRF-ELEC Model

Mengyu Sun[1,5], Dongxia Liu[1], Xiushu Qie[1], Edward R. Mansell[2], Yoav Yair[3], Alexandre O. Fierro[2,4], Shanfeng Yuan[1], Zhixiong Chen[1,5], Dongfang Wang[1]

[1] Key Laboratory of Middle Atmosphere and Global Environment Observation, Institute of Atmospheric Physics, Chinese Academy of Sciences, Beijing, China

[2] NOAA/National Severe Storms Laboratory, Norman, Oklahoma, USA

[3] Interdisciplinary Center (IDC) Herzliya, School of Sustainability, Herzliya, Israel

[4] Cooperative Institute for Mesoscale Meteorological Studies, University of Oklahoma, Norman, Oklahoma, USA

[5] College of Earth and Planetary Sciences, University of Chinese Academy of Sciences, Beijing, China

Correspondence to: Dongxia Liu (liudx@mail.iap.ac.cn)

Abstract

To investigate the effects of aerosol on lightning activity, the Weather Research and Forecasting (WRF) Model with a two-moment bulk microphysical scheme and bulk lightning model was employed to simulate a multicell thunderstorm that occurred in the metropolitan Beijing area. The results suggest that under polluted condition lightning activity is significantly enhanced during the developing and mature stages. Electrification and lightning discharges within the thunderstorm show distinguish characteristics by different aerosol conditions through microphysical processes. Elevated aerosol loading increases the cloud droplets numbers, the latent heat release, updraft and ice-phase particle number concentrations. More charges in the upper level

are carried by ice particles and enhance the electrification process. A larger mean-mass radius of graupel particles further increases non-inductive charging due to more effective collisions. In the continental case where aerosol concentrations are low, less latent heat releases in the upper parts and as a consequence, the updraft speed is weaker leading to smaller concentrations of ice particles, lower charging rates and less lightning discharges.

1 Introduction

Lightning activity is related to two important factors: dynamic-thermodynamic and microphysical characteristics (e.g. Williams et al., 2005; Guo et al., 2016; Wang et al., 2018; Zhao et al., 2020). Since the dynamic-thermodynamic processes affect the development of thunderstorm significantly, lightning activity is influenced by various dynamic-thermodynamic variables: temperature (Price, 1993), relative humidity in the lower and middle troposphere (Xiong et al., 2006; Fan et al., 2007), and convective available potential energy (Qie et al., 2004; Stolz et al., 2015), and many others.

The impacts of aerosol on the development of thunderstorm especially in metropolitan areas have been researched extensively. Observational studies indicated that the enhancement of lightning activity was related to increased cloud condensation nuclei (CCN) concentration (e.g., Westcott, 1995; Orville et al., 2001; Kar et al., 2009; Wang et al., 2011; Chaudhuri and Middey, 2013; Thornton et al., 2017; Yair, 2018; Qie et al., 2021). Kar et al. (2009) found a positive correlation between PM10 and SO_2 concentration and lightning flash densities around major cities in South Korea. A positive relationship between levels of particle pollution and lightning flash counts was also indicated by Chaudhuri and Middey (2013).

Furthermore, a variety of numerical simulations (e.g., Mitzeva et al., 2006) demonstrated the effects of aerosol on enhancing lightning activity. Using the Weather Research and Forecasting (WRF) Model with explicit spectral bin microphysics, Khain et al. (2010) found elevated aerosol increased the number of cloud droplets and the release of latent heat by acting as CCN. Therefore, more liquid water was lifted to

mixed-phase region by strong updrafts, with more ice-phase particles produced which can affect charge separation and lightning formation (Takahashi, 1978; Saunders and Peck, 1998; Takahashi et al., 1983; Mansell et al., 2005; Yair, 2008; Yair et al., 2021). Mansell and Ziegler (2013) suggested that greater CCN concentration led to greater lightning activity up to a point by testing a wide range of CCN concentration in a 3D model with two-moment bulk microphysics and stochastic branched discharge parameterization (Mansell et al., 2002). They also noted that average graupel density stayed high at lower CCN, but dropped at higher CCN because smaller droplets caused lower rime density. Zhao et al. (2015) showed that enhancing aerosol concentration resulted in an enhancement of electrification processes, due to the increasing growth rate of snow and graupel particles. However, Tan et al. (2017) simulated a thunderstorm in Changchun city with a 3D cumulus model coupled with aerosol module, electrification and lightning discharge, showing that the ice crystal and graupel number increased while the graupel mixing ratio decreased as the aerosol concentration increased.

The microphysical processes under different CCN concentration, especially the initiation and growth of ice-phase particles varied from different simulation studies. There are few studies that discussed the aerosol effects on thunderstorm with explicit electrification and discharge parameterization in the model simultaneously (e.g., Mitzeva et al., 2006; Mansell and Ziegler, 2013; Zhao et al., 2015). The detailed effects of aerosol on the discharging need further study.

By analyzing lightning data from the Beijing Lightning Network (BLNET) and $PM_{2.5}$ (particulate matter with aerodynamic diameter less than or equal to 2.5 μm) data, Sun et al. (2020) found a positive relationship between flash counts and $PM_{2.5}$ concentration prior to the occurrence of thunderstorm. As a mega city, Beijing has higher aerosol concentration resulting from anthropogenic air pollution. Still, the effects of aerosol on both electrification and discharges have been rarely discussed in this area by numerical simulation. Therefore, in this paper we present sensitivity studies on how the different CCN concentration influence the characteristic of thundercloud over the metropolitan Beijing area using the WRF-ELEC (Fierro et al., 2013). We conducted

sensitivity studies to evaluate the response of the microphysical properties, as well as electrification and lightning processes to aerosol characteristics. This paper is organized as follows: section 2 describes the data and methodology used in the study, section 3 introduces the design of simulations, section 4 presents the results, and section 5 discusses and summarizes the study.

2 Data sources

2.1 Observational dataset

Total flash numbers were obtained from the Beijing Lightning Network (BLNET), which consists of 16 stations covering East-West 110 km and North-South 120 km areas since 2015 (refer to Figure 1). The BLNET provides 3D-location results of flashes, including both intra-cloud (IC) and cloud-to-ground (CG) lightning (Wang et al., 2016). The average detection efficiency of the BLNET is 93.2% for the total flashes (Srivastava et al., 2017). In this study, the 3D-location lightning radiation pulses were grouped in flashes based on the criteria of 400 ms and 15 km. This grouping criteria was modified from the algorithm in Srivastava et al. (2017). In section 3, the lightning frequency from BLNET was calculated in every 6 min intervals, corresponding to the time span of Doppler radar scanning. In addition, the radar reflectivity data was obtained from an S-band Doppler radar (Chinese CINRAD/SA) near Beijing urban area (39.81 °N, 116.47 °E), and were updated every 6 min. The vertical levels vary from 500 m to 20 km and were processed into composite radar reflectivity with a horizontal resolution (0.01 °×0.01 °). The precipitation data are taken from 295 gauge stations in a weather monitoring network of automatic weather stations in the Beijing region (refer to Figure 1), with spacing of approximately 3 km in urban area. The real-time hourly average ground levels of $PM_{2.5}$ are from the China National Environmental Monitoring Center (http://106.37.208.233:20035/ accessed on 2 May 2021).

2.2 Synoptic background

A mesoscale convective system over the Beijing area influenced by a strong Mongolia cold vortex on 11 Aug 2017 was simulated in this study. Based on the weather map at 00:00 UTC (figure not shown), there was a prevailing westward airflow in the south of the cold vortex, which brought dry cold air in middle layer. At low-level of 850 hPa, the southwesterly jet transported warm and humid air mass, forming an unstable condition together with cold air mass above. The sounding profile over Beijing (39.9 °N, 116.2 °E) exhibited an unstable thermodynamic condition for thunderstorm initialization, as shown in Figure 2, with a surface-based convective available potential energy (CAPE) of 3937 J kg^{-1} at 12:00 UTC. The special terrain condition with mountain in the northwest and ocean in the southeast (Qie et al., 2020), as well as heat island effect and elevated aerosol loading in the urban region (Zhang et al., 2013; Liu et al., 2018), likely enhanced the convection and were responsible for the occurrence of heavy rainfall and large hail as well as intensive lightning activity in the Beijing area. According to the surface-based automatic weather observation network in Beijing, the average rainfall in the urban area and the eastern region was 10-30 mm, with locally exceeding 100 mm. The total lightning flashes of this case accounted for one-third of the total number of lightning flashes during the 2017 warm season (Chen et al., 2020).

3. Model overview

The WRF Model (version 3.9.1) coupled with bulk lightning model (BLM, Fierro et al., 2013) and a two-moment bulk microphysics scheme (Mansell et al., 2010; Mansell and Ziegler, 2013) was used to simulate the multicell thunderstorm that occurred on 11 August 2017 in the Beijing metropolitan area.

The simulations employ the two-moment bulk microphysics scheme of Mansell et al. (2010), which predicts both mass mixing ratio and number concentration for a range of hydrometeor species (droplets, rain, ice crystals, snow, graupel, and hail). Microphysical processes include cloud droplet nucleation, condensation, collection-

coalescence, riming, ice multiplication, freezing and melting, and conversion between different hydrometeors, etc. It is noted that the predicted graupel density is variable, which makes it possible for the single graupel category to represent a range of particles from high-density frozen drops to low-density graupel (Mansell et al., 2010). The graupel growth processes contain collection of ice crystals by graupel, collection of snow particles by graupel, deposition of vapor to graupel, collection of supercooled water (cloud droplets and/or raindrops) by graupel, and conversions between hydrometeors. Further details of the interactions among particles can be found in Mansell and Ziegler (2013), Mansell et al. (2010), and Ziegler (1985). The CCN concentration is predicted as a bulk activation spectrum and initially mixed well vertically, following Eq. (1) of Mansell et al. (2010):

$$N_{CCN} = CCN \times S^k, \quad (1)$$

where *CCN* is the assumed CCN concentration, S is the supersaturation with respect to liquid water, and k = 0.6. The initiation of cloud droplets (both for cloud base and in-cloud) is based on Twomey (1959) and adjusted by Mansell et al. (2010).

Explicit charging physics includes both non-inductive charging (Saunders and Peck, 1998) and inductive or polarization charging (Ziegler et al., 1991). We employed non-inductive electrification scheme described by Saunders and Peck (1998) and adjusted by Mansell et al. (2005) in this study. The magnitude of charge separated within a grid cell (δq) is calculated from the non-inductive critical charging curve as a function of temperature and riming accretion rate (*RAR*), following Eq. (2) of Mansell et al. (2005):

$$\delta q = B D_{n,1}^{a} \left(\overline{V}_g - \overline{V}_I\right)^b q_{\pm}(RAR), \quad (2)$$

where *B*, *a*, *b* are a function of crystal size; $D_{n,1}^{a}$ is the mean volume diameter of the ice crystal-snow, $\overline{V}_g$ and $\overline{V}_I$ are the mass-weighted mean terminal fall speeds for graupel and ice crystal; the $q_{\pm}(RAR)$ is the charge separation as a function of the *RAR* from Brook et al. (1997) adjusted by Mansell et al. (2005). Non-inductive (i.e., independent of external electric fields) charge separation resulting from rebounding collisions between various ice-phase particles (ice, graupel, snow, hail) are all

parameterized based on results obtained from laboratory experiments (Takahashi, 1978; Saunders et al., 2001; Mansell et al., 2005). Inductive charging requires a pre-existing electric field to induce charge on the surfaces of the colliding particles (Mansell et al., 2005). Numerical experiments (Mansell et al., 2010) found that total inductive charging, is about an order of magnitude weaker than non-inductive charging, but can be important for lower charge regions. Only collisions between cloud droplets and ice-phase particles (graupel, ice, hail) are considered for inductive electrification. The electric field is simulated by solving Poisson equation for the electric potential Φ:

$$\nabla^2\Phi = -\frac{\rho_{tot}}{\varepsilon}, \quad (3)$$

where ρ_{tot} is the net space charge and ε is the electric permittivity of air (8.8592×10^{-12} F/m). A message-passing-interface (MPI) black box multigrid iterative solver or BoxMG algorithm (Dendy, 1987) is extended to solved Eq. (3). And then the three components of the electric field and its magnitude are computed from Eq. (4):

$$E = -\nabla\Phi, \quad (4)$$

The discharge model parameterization from Ziegler and MacGorman (1994) is used within a cylindrical region (Fierro et al., 2013). A flash would be initiated when the electric field exceeds a breakdown threshold, which variants of vertical electric profile of Dwyer (2003) at a model grid point (from here on, we shall use the term 'grid points' for short). A discharge is centered at the initiation grid points within a cylinder of extending vertically through the depth of the domain. If the space charge magnitude at a grid point exceeds a specific space charge threshold (0.1 nC $\cdot$m^{-3} herein), this grid point will be involved in discharge within the cylinder during this time step. After each discharge, the charge magnitude is set to 70% (Rawlins, 1982; Ziegler and MacGorman, 1994) of the summed magnitude for all grid points. Then the charges will be redistributed throughout all discharge volumes and the electric field is be recalculated. The discharge in each time step will be terminated until the maximum electric field no longer exceeds the breakdown threshold. An estimate of flash origin density (*FOD*) rate (over a time period $T = t_2 - t_1$) is computed following Eq. (5):

$$FOD(T) = \frac{G}{C}\int_{t_1}^{t_2} B(t)dt, \quad (5)$$

where G is the horizontal grid cell area, C the cylinder cross sectional area (set in the following simulations to radius R = 12 km (Fierro et al., 2013)). In this study, the integral represents the sum of flashes $[B(t)]$ that extend into the grid column for all the time steps within the time period *T*. Further, flash extent density (*FED*) are given by Eq. (6). Thus, the predicted flash extent density over the Beijing area in section 3 is the *FED* calculated in 6 min intervals:

$$FED(T) = \sum FOD(T). \quad (6)$$

3.1 Design of the simulations

The nested model configuration for the simulations are shown in Table 1. The WRF-ELEC model is configured by a two-way interactive nested domain. The outer domain has a horizontal grid spacing of 6 km (442 ×391 grid points) and the inner domain is 2 km (496 ×496 grid points), both centering at (40 °N, 116.05 °E). The number of vertical levels are 40 and the top is set to 50 hPa for the two domains. The model physics configuration is the Unified Noah Land Surface Model (Chen and Dudhia, 2001). The longwave and shortwave radiation are parameterized following the Rapid Radiation Transfer Model (Mlawer et al., 1997) and the Dudhia scheme (Dudhia, 1989), respectively. The Bougeault-Lacarrere PBL scheme is used to parameterize the boundary layer processes (Bougeault and Lacarrere, 1989). Simulations began at 00:00 UTC on 11 August 2017 and integrated for 24 h. The period of interest was from 09:00 UTC until 17:00 UTC (time in the simulations). The 3-hourly NCEP GFS (Global Forecast System) data with 0.5 °×0.5 ° resolution are used to establish the initial and boundary conditions.

To survey the aerosol effects on the structure of thunderstorm and lightning activity, two sensitivity experiments are performed with different CCN concentration: a polluted case (P-case) and a continental case (C-case). Figure 3 shows hourly average mass concentration of $PM_{2.5}$ on 11 August 2017. The hourly-average value of the observed $PM_{2.5}$ concentration before the thunderstorm initiation (more than 110 μg m^{-3}

^{3}) is much higher than the 3-year mean $PM_{2.5}$ concentration (69.4±54.8 μg m^{-3}) in the Beijing area (Liu et al., 2018). Therefore, the CCN concentration is selected as the P-case which is consistent with observation. The initial value for the P-case is set as a number mixing ratio relative to sea level air density ρ_0: $2000/\rho_0 \times 10^{-6}$ kg^{-1}, where ρ_0=1.225 kg m^{-3}, and the local number concentration is $2000 \times (\rho_{air}/\rho_0)$ cm^{-3}. And the initial number concentration for the C-case is set at $1200 \times (\rho_{air}/\rho_0)$ cm^{-3}, consistent with typical continental conditions (e.g. Hobbs and Rangno, 1985; Mansell et al., 2005; Mansell, personal communication, 2019). The relatively high prescribed CCN concentration guaranteed small droplet diameters and should be effectively delayed the warm rain process in the model (Mansell and Ziegler, 2013).

4 Results

4.1 Radar reflectivity, precipitation and lightning flashes of multicell

Figure 4 shows the observed and simulated radar reflectivity at different periods for both cases, with the formation of thunderstorms in the simulation earlier than the observation about 1.5 h. For this reason, we display the simulation and observation with ~90 minutes time difference. It is clear that both simulated times in the P-case exhibit an overall good agreement with the evolution and morphology of the radar echo, especially evidenced by the northeast-southwest orientation of the radar echo at 11:54 UTC in the simulated polluted case (13:24 UTC in the observation). We also present the comparison of radar reflectivity as a function of height from the observation and simulations in the corresponding periods (Figure 5). According to the morphology and intensity of the radar echo, the observed radar reflectivity is in better agreement with simulated radar reflectivity only in the polluted case. Note that the modeled reflectivity differs from the observation in the northwestern area (115.4 °E-116.0 °E, Fig. 4a, 4c and 4e), the impacts of aerosol on lightning activity will only be evaluated in the southeastern Beijing area (39.4 °N-40.6 °N, 116.0 °E-117.5 °E, shown in Fig. 4d; here on, 'domain' for short).

Precipitation measurements from around 300 gauge stations in the Beijing area are compared with the WRF simulations. Figure 6 shows hourly peak rainfall rate from the rain gauges and from simulations for the P-case and C-case. As noted, the formation of thunderstorm in the simulations occurring about 1.5 h earlier than in the observation. So we display the simulations and observation with a 1 h time shift. It can be seen that the peak rainfall rate reaches the maximum at the same stage of development in both simulations (at 12:00 UTC) and the measurement (at 13:00 UTC). The rainfall in the P-case continues for around 9 hours, which is consistent with the gauge measurement, while the rainfall in the C-case lasts one hour less than the observation. The maximal peak rainfall rate in the P-case is 97.3 mm/h, which is larger than the measurement (and the C-case) with a value of 80 mm/h (77.3 mm/h). The difference in the rainfall rate is further analyzed through the comparison of spatial distribution of precipitation. Figure 7 displays the 6-hourly accumulated precipitation from the observation (11:00-17:00 UTC) and from the simulations for the P- and C-case (10:00-16:00 UTC). Both the simulations reproduce the precipitation in the southeastern region, where the gauge measurements show the accumulated rainfall are exceeding 100 mm. The coverage of the simulated precipitation in the P-case extends to the northeast area compared to the C-case, which is more consistent with the observation. This area is included in our analyzed region shown in Figure 4d.

The temporal variation of total flashes from BLNET is shown in Figure 8a, including both intra-cloud (IC) and cloud-to-ground (CG) lightning. The lightning frequency gradually increased during 11:00-12:00 UTC and raised significantly after 12:00 UTC, as well as reached the peak value at 12:30 UTC, and then decreased gradually. According to the evolution of radar reflectivity and lightning activity (Van Den Broeke et al., 2008; Kumjian et al., 2010, Liu et al., 2021), the real and simulated developments of the thunderstorm are shown in Table 2. The temporal evolution of predicted FED over Beijing area under the polluted and continental cases are shown in Fig. 8b, both of them start earlier than observation about 1.5 h. Compared to the continental case, the variation of predicted flashes under polluted condition is better consistent with the observation. The predicted FED for the P-case and measured flashes

increase significantly after 10:00 UTC (11:30 UTC in the observation), and reach the peak around 11:00 UTC (12:30 UTC in the observation). In contrast, the predicted flashes for the C-case reaches the peak around 10:30 UTC, earlier than the P-case and measured lightning flashes, and then decreases dramatically. Within the duration of the thunderstorm, the overall FED in the polluted case is noticeably about 50% higher than the C-case.

Figure 9 displays the number of initiations over the Beijing area for the C-case and P-case during different periods. To examine the details of lightning response to aerosol, the intensity of lightning activity can be categorized into four levels by the lightning grid points in each time step: light (50-100 grid points), moderate (100-200 grid points), heavy (200-300 grid points) and extreme (>300 grid points). Then the number of points (grid columns) in each category is counted hourly as the 'number of initiations'. A comparison of the different lightning intensity categories reveals that the simulated lightning activities increase during 10:30-12:30 UTC (Fig. 9b and 9c) under high aerosol loading, corresponding to the developing and mature stages of the thunderstorm. During 09:30-10:30 UTC, while different categories of lightning intensity are enhanced for both P- and C-case (Fig. 9a), it is noted that the maximum lightning initiation occurs in the extreme level for the P-case. In the dissipating stage, lightning activities decrease dramatically in the P- and C-case (Fig. 9d), but the lightning intensity under polluted condition is still stronger compared to the C-case. Hence, the results indicate that elevated aerosol loading enhances lightning activities especially in the developing and mature stages of thunderstorm. In the following contents we will offer a possible explanation for this effect.

4.2 Microphysical properties of multicell

To investigate the effects of aerosol on lightning activities, we first analyze the simulated microphysical properties in both the continental and polluted sensitivity studies. Figure 10a-10h show the temporal variations of the vertical profiles for

different hydrometeors. For each quantity, the mass mixing ratio and number concentration of hydrometeors are averaged horizontally over the analyzed region at a given altitude. The domain-averaged microphysical properties for the various hydrometeors are summarized in Table 3. The domain-average mean-mass $radius_h$ of hydrometeors in Table is calculated following Eq. (7):

$$radius_h = [\frac{1}{c_h} \times \frac{Sum(\rho_{air}(i,j,k) \times q_h(i,j,k))}{Sum(\rho_{air}(i,j,k) \times n_h(i,j,k))}]^{1/3}, \quad (7)$$

where ρ_{air} is the air density, and c_h, q_h, n_h are the density, mass concentration, and number concentration of hydrometeor species h (Mansell et al., 2010), respectively. Figure 10i-10j display the time-height plots of maximum radar reflectivity and vertical velocities. The related convective properties are shown in Table 4.

It can be seen that elevated aerosol loading results in increasing cloud droplet concentrations (Figure 10b and Table 3). Under polluted condition, more aerosols could be activated into cloud droplets and more water vapor condenses onto these droplets, leading to large cloud water content and small droplet size (Lynn et al., 2007; Wang et al., 2011; Zhao et al., 2015; Jiang et al., 2017). Thereby, relatively more latent heat of condensation released in the P-case where large cloud water content exists, which can be seen in the vertical distribution of peak latent heat (Figure 12). The temporal variation of domain-averaged mean-mass radius for cloud droplets is shown in Figure 11. Under polluted condition, cloud droplets with smaller mean-mass radius are too small to be converted into raindrops. As a consequence, the rainwater mass mixing ratio is less in the polluted case compared to the continental one (Figure 10d). Instead, these cloud droplets could be transported to higher levels (< -40 ℃) by the strong updrafts resulting from increased latent heat. Previous studies showed that larger vertical velocities were driven by increased microphysical latent heating. (Wang et al., 2011; Mansell and Ziegler, 2013; Altaratz et al., 2017; Fan et al., 2018; Li et al., 2019). As shown in Table 4, the maximum updraft in the P-case (53.5 m/s) occurs above 12 km, while the height of maximum velocity for the C-case (50.4 m/s) is 10.5 km. As a result, the mixed-phase processes are enhanced and there are more ice crystals in the P-case above 10 km (Figure 10h). Observations and simulations also found that the content of

ice crystals could be greater under polluted condition, resulting from more condensation latent heat and strengthened updrafts (Khain et al., 2008; Koren et al., 2010; Wang et al., 2011; Zhao et al., 2015; Tan et al., 2017; Lynn et al., 2020). The number concentration of ice crystals is much larger under polluted condition (Table 3), with domain-average of 3850×10^3 kg^{-1} for the polluted case and 2280×10^3 kg^{-1} for the continental case. The size of raindrops in the P-case is larger, which is also be found in Wang et al. (2011), probably due to the melting of ice-phase particles. These differences between cloud, rain droplets and ice crystals are directly influenced by the increasing aerosol loading. It is worth noting that the maximum of peak latent heat in the P-case occurs above 10 km at 09:30 UTC (Figure 12), indicating that more cloud droplets are lifted to the upper levels (< -40 °C) and converted into ice crystals at the beginning stage of the thunderstorm. As noted, the latent heat shown in Figure 12 results from both condensation and freezing. The high value of latent heat existed in the higher levels (above 10 km) reveals a large amount release of frozen latent heat. Previous studies also found that elevated aerosol loading contributed to the increasing of frozen latent heat (e.g., Khain et al., 2005; Lynn et al. 2007; Storer et al., 2010; Li et al., 2017). The increased frozen latent heat during this period, together with relatively enhanced condensation latent heat, further ensure vigorous vertical growth and lead to the maximum updraft occurred at 10:48 UTC in the P-case.

In contrast, the domain-averaged mass mixing ratio of graupel is relatively less in the P-case (Figure 10e and 10f). Less graupel content under polluted condition is rather surprising, since previous simulation studies (Wang et al., 2011; Zhao et al., 2015) found that there could be more graupel at the mature stage of thunderstorm, by virtue of enhanced convection and more cloud droplets lifted to the mixed-phase region. These could happen if starting from a much lower CCN concentration (< 400 cm^{-3}), in this study, with higher CCN concentration (> 1000 cm^{-3}), the reduced raindrop freezing (Fig. 10d) probably explains the lower density of graupel. Smaller fall speed of the lower density graupel further lead to less riming and graupel contents. Other simulation also found a decrease of graupel mixing ratio under polluted conditions, and partly attributed the decrease to the melting of graupel particles (Tan et al., 2017). In this study, the

graupel content was higher in the C-case, probably owing to higher rainwater content and corresponding raindrop freezing. It is worth noting that the number concentration of graupel in the polluted case is rather less compared to the continental one (Table 3), with 12 kg^{-1} for the P-case, and 28 kg^{-1} for the C-case, respectively. Such a phenomenon could offer a partial explanation for the graupel of larger mean-mass radius appearing in the P-case (Figure 11c and Table 3). The domain-averaged mean-mass radius of graupel reaches 479.5 μm for the P-case, compared to 322.4 μm for the C-case. In contrast to the small difference in mean-mass radius of ice crystals between the polluted and continental cases (Figure 11d), the radius of graupel is much larger in the P-case. This likely results in a larger collision efficiency between graupel and other ice-phase particles, enhancing non-inductive charging.

Increasing aerosol loading affects the key microphysical processes, especially in the ice-phase processes yielding to larger ice crystal content/mass and larger graupel size. Both of them would inevitably affect lightning activity by affecting the rate and magnitude of charge separated during ice-graupel collisions.

4.3 The relationship between electrification, microphysics and dynamics

The time series of the peak positive (negative) charge density in the two cases are shown in Figure 13. The domain-averaged peak charge structure in the P-case is similar to that of the C-case before 12:00 UTC, with positive charge region distributed above the negative charge region. In both cases, the maximum peak positive charge density occurs above 8.5 km (< -30 °C). While the peak charge density for the polluted case is significantly greater, especially at the developing and mature stages (10:00-12:00 UTC). The peak positive charge density for the P-case is more than +4 nC m^{-3} during this period, but the peak charge density is less than +2 nC m^{-3} in the C-case. With the development of the thunderstorm, the charge density decreases gradually for both cases. At the upper levels, the peak charge density is still greater and lasts longer under polluted condition.

To analyze the relationship between hydrometeors and electrification, vertical cross sections are shown in Figure 14a and 15a, which display the total charge distribution at the mature stage of the thunderstorm in the polluted (11:54 UTC) and continental cases (11:24 UTC), respectively. It is noted that the vertical profiles of the charge distribution are more detailed than the domain-averaged charge structure shown in Figure 13. The charge structure with positive charge in the upper levels and negative charge in the lower levels was simulated in the C-case. There were positive charge appeared in the lower negative charge center (Fig. 15a), which means that this charge structure is a little different from the normal dipole (upper charge positive, lower charge negative; e.g., Thomas et al., 2001). While the positive charge magnitude in the lower levels for the C-case is relatively small to form normal tripole, in which a dominant region of negative charge with positive charge above and a positive charge below with approximately the same order of magnitude of charge (Simpson and Scrase, 1937; William et al., 1989). In the polluted case, with a negative charge region in the upper level (above 13 km), the updraft region exhibited an charge structure with a positive charge center located in the middle, and two negative charge centers in the upper and lower levels; e.g. Mansell et al., 2005). For the total net space charge density, the maximum of positive charge density at the mature stage in the P-case is up to +1 nC m^{-3}, which is much higher than that in the C-case (less than +0.5 nC m^{-3}).

We attempt to explain the origins of the charge distribution by examining the polarity and amount of charge carried by different hydrometeor species (namely by ice, graupel, snow and hail particles). The negative charge region in the upper levels (12-15 km) for the P-case resulted from collisions of graupel particles with smaller ice crystals and snow particles (Fig. 14d), with the 30 dBZ echo tops reaching 13 km. The simulated vertical distribution of net charge in the C-case was caused by ice and snow particles charged positively at 8-12 km and graupel particles charged negatively at 4-7 km, respectively (Fig. 15b and 15d). The collisions between graupel and hail particles could partially explain the intense positive charge center located at 8-12 km in the P-case. Less ice-phase particles appear in upper level in the continental case compared to the polluted one, corresponding to a relatively weaker charge center. Figure 14c and 15c

show the cross sections of the simulated radar reflectivity and vertical velocity at 11:54 UTC (11:24 UTC) under different aerosol conditions. It is evident that both updraft and downdraft for the polluted case are greater than that for the continental one at higher levels, resulting from more frozen latent heat, and as a consequence, the total charge density is significantly greater above 12 km.

According to Saunders and Peck (1998) non-inductive charging curve, graupel charged negatively within regions of relatively weak updrafts (< 5 m s^{-1}) and lower liquid water content (LWC), forming a negative charge region at 4-8 km in the P-case (Fig. 14a and 14d). With higher LWC in the polluted case, graupel, ice and hail were charged positively, forming a strong positive charge center at 9km (< -20 ℃), as shown in Fig. 14a. The simulations show that non-inductive charging mechanism plays a main role at the mature stage, the rate of which is one order of magnitude larger than inductive charging (Fig. 16). As described in section 4.2, more ice particles and graupel with larger radius appeared at this stage in the P-case, evidenced by the larger simulated radar reflectivity (Fig. 14c), and the ensuing collision rates led to significantly stronger non-inductive charging at 6-10 km (Fig. 16b). In consequence, it is obvious in the Figure 14a and 15a that the charge density for the P-case is much higher than the C-case, indicating that aerosol plays an important role in affecting the accumulated charge density through microphysical and further electrical processes.

The appearance of more ice-phase particles in upper level, increasing ice crystal number and mean-mass radius of graupel particles, together led to greater charge densities and as a consequence to stronger electric field intensities. Lightning discharge in the WRF-ELEC occurs if the electric field magnitude exceeds a prescribed, fixed threshold, which further supports the important role of aerosols in enhancing storm electrification. Mansell et al. (2013) found that greater CCN concentration led to increased lightning activity up to a point, by affecting microphysical and electrical characteristics, with a large sensitivity to ice multiplication. In agreement with Mansell et al. (2013), this study showed that higher CCN concentration in the polluted case resulted in a relatively strong upper charge region, together with increased charge density and electric field intensity, finally enhancing lightning activity, as shown in

Figure 8b.

5 Conclusions and discussion

To elucidate the effects of aerosol on lightning activity, a two-moment bulk microphysics scheme (Mansell et al., 2010; Mansell and Ziegler, 2013) and bulk lightning model (BLM, Fierro et al., 2013) were coupled in the WRF model to simulate a multicell thunderstorm that occurred on 11 August 2017 in the metropolitan Beijing area. The simulated distributions and spatio-temporal development of radar reflectivity and precipitation under polluted condition are in overall agreement with observations.

Sensitivity experiments show that the intensity and duration of lightning activity are evidently different between moderate (continental) and high (polluted) aerosol concentrations, resulting from microphysical processes. Elevated aerosol concentrations lead to increasing cloud droplet contents and smaller droplet size. Smaller droplets suppress collection/coalescence processes and lead to the less rainwater under polluted condition. These cloud droplets which could not accreted by raindrops will be transported to higher levels and convert into ice crystals. Increased latent heat release leads to strong updrafts, and in turn more cloud droplets could be lifted up. As a result, the ice crystal contents are much greater in the P-case. Although the graupel contents are relatively less under polluted condition resulting from less raindrop freezing, the radius of graupel is much larger in the P-case due to much less number concentration. Consequently, elevated aerosol loading enhances the development of ice-phase microphysical processes, evidenced by more ice crystals and larger radius of graupel participating in charge-separation and electrification processes. Non-inductive charging increases due to more frequent and effective collisions between graupel and other ice-phase particles. These bring about higher charge density, together with larger upper charge region caused by more ice-phase particles lifted to higher levels, leading to electric field magnitudes which exceed the breakdown threshold value, eventually culminating in an enhanced lightning activity. During the developing and mature stages of the thunderstorm, the latent heat release at higher altitude is noticeably

greater in the P-case, mainly due to the release of frozen latent heat from supercooled liquid particles.

Observation and simulation studies found that elevated aerosol loading enhanced the electrical activity (e.g., Koren et al., 2010; Wang et al., 2011). Some previous studies suggested that the mass mixing ratio of ice and graupel increased with the enhanced CCN concentration, eventually resulting in stronger lightning activity (e.g., Wang et al., 2011; Zhao et al., 2015), while a decrease of graupel mixing ratio was found by Tan et al. (2017). It should also be noted that when aerosol concentrations are too large, this leads to the inhibition of convection resulting in less lightning, as discovered by Altaratz et al. (2010) in the Amazon basin, as well as by Hu et al. (2019) in Houston region, and simulated by Mansell and Ziegler (2013). In this study, we found the lightning activity enhanced under polluted condition resulting from increasing ice crystal number and radius of graupel particles. More ice-phase particles existed at upper levels under polluted condition, forming a relatively strong charge region, which is also indicated by Zhao et al. (2015).

The impacts of aerosol on lightning were investigated acting as CCN, however, aerosol also tends to affect electrification and lightning discharge by acting as ice nuclei (IN) through microphysical processes (Tao et al., 2012; Fan et al., 2017). More sensitive experiments are still needed to discuss the influences of aerosol on lightning due to microphysical and thermodynamic processes, acting as IN.

Data availability

To request the data given in this study, please contact Dr. Dongxia Liu at the Institute of Atmospheric Physics, Chinese Academy of Sciences, via email (liudx@mail.iap.ac.cn).

Author contributions

MS, XQ designed the research ideas for this study. MS carried the study out and

prepared the paper. EM provided analysis ideas for the microphysics and electrification. DL, YY and AF edited the paper. Other co-authors participated in science discussions and article modification.

Competing interests

The authors declare that they have no conflict of interest.

Acknowledgment

This research was supported by an NSFC-ISF grant (Nos. 41761144074, 2640/17), and the National Natural Science Foundation of China (Nos. 41630425, 41875007).

Reference

Altaratz O, Kucienska B, Kostinski A B, et al. Global association of aerosol with flash density of intense lightning[J]. Environmental Research Letters, 2017, 12(11).

Altaratz O, Koren I, Yair Y, et al. Lightning response to smoke from Amazonian fires[J]. Geophysical Research Letters, 2010, 37(7).

Bougeault P, Lacarrere P. Parameterization of orography-induced turbulence in a mesobeta--scale model[J]. Monthly weather review, 1989, 117(8): 1872-1890.

Brooks I M, Saunders C P R, Mitzeva R P, et al. The effect on thunderstorm charging of the rate of rime accretion by graupel[J]. Atmospheric Research, 1997, 43(3): 277-295.

Chaudhuri S, Middey A. Effect of meteorological parameters and environmental pollution on thunderstorm and lightning activity over an urban metropolis of India[J]. Urban Climate, 2013, 3: 67-75.

Chen Z, Qie X, Yair Y, et al. Electrical evolution of a rapidly developing MCS during its vigorous vertical growth phase[J]. Atmospheric Research, 2020, 246: 105201.

Chen F, Dudhia J. Coupling an advanced land surface–hydrology model with the Penn

State–NCAR MM5 modeling system. Part I: Model implementation and sensitivity[J]. Monthly weather review, 2001, 129(4): 569-585.

Dendy, Jr J E. Two multigrid methods for three-dimensional problems with discontinuous and anisotropic coefficients[J]. SIAM journal on scientific and statistical computing, 1987, 8(5): 673-685.

Dudhia J. Numerical study of convection observed during the winter monsoon experiment using a mesoscale two-dimensional model[J]. Journal of Atmospheric Sciences, 1989, 46(20): 3077-3107.

Dwyer J R. A fundamental limit on electric fields in air[J]. Geophysical Research Letters, 2003, 30(20).

Dye J E, Knight C A, Toutenhoofd V, et al. The Mechanism of Precipitation Formation in Northeastern Colorado Cumulus III. Coordinated Microphysical and Radar Observations and Summary[J]. Journal of the Atmospheric Sciences, 1974, 31(8): 2152-2159.

Fan J, Rosenfeld D, Zhang Y, et al. Substantial convection and precipitation enhancements by ultrafine aerosol particles[J]. Science, 2018, 359(6374): 411-418.

Fan J, Leung L R, Rosenfeld D, et al. Effects of cloud condensation nuclei and ice nucleating particles on precipitation processes and supercooled liquid in mixed-phase orographic clouds[J]. Atmospheric Chemistry and Physics, 2017, 17(2).

Fan J, Zhang R, Li G, et al. Effects of aerosols and relative humidity on cumulus clouds[J]. Journal of Geophysical Research: Atmospheres, 2007, 112(D14).

Fierro A O, Mansell E R, Mac Gorman D R, et al. The implementation of an explicit charging and discharge lightning scheme within the WRF-ARW model: Benchmark simulations of a continental squall line, a tropical cyclone, and a winter storm[J]. Monthly Weather Review, 2013, 141(7): 2390-2415.

Guo J, Deng M, Lee S S, et al. Delaying precipitation and lightning by air pollution over the Pearl River Delta. Part I: Observational analyses[J]. Journal of Geophysical Research: Atmospheres, 2016, 121(11): 6472-6488.

Hobbs P V, Rangno A L. Ice Particle Concentrations in Clouds[J]. Journal of the Atmospheric Sciences, 1985, 42(23): 2523-2549.

Hu J, Rosenfeld D, Ryzhkov A, et al. Polarimetric radar convective cell tracking reveals large sensitivity of cloud precipitation and electrification properties to CCN[J]. Journal of Geophysical Research: Atmospheres, 2019, 124(22): 12194-12205.

Jayaratne E R, Saunders C P R, Hallett J. Laboratory studies of the charging of soft-hail during ice crystal interactions[J]. Quarterly Journal of the Royal Meteorological Society, 1983, 109(461): 609-630.

Jiang M, Feng J, Sun R, et al. Potential influences of neglecting aerosol effects on the NCEP GFS precipitation forecast[J]. Atmospheric Chemistry and Physics, 2017, 17(22):13967-13982.

Kar S K, Liou Y A, Ha K J. Aerosol effects on the enhancement of cloud-to-ground lightning over major urban areas of South Korea[J]. Atmospheric Research, 2009, 92(1):0-87.

Khain A, Rosenfeld D, Pokrovsky A. Aerosol impact on the dynamics and microphysics of deep convective clouds[J]. Quarterly Journal of the Royal Meteorological Society: A journal of the atmospheric sciences, applied meteorology and physical oceanography, 2005, 131(611): 2639-2663.

Khain A, Cohen N, Lynn B, et al. Possible Aerosol Effects on Lightning Activity and Structure of Hurricanes[J]. Journal of the Atmospheric Sciences, 2008, 65(12):3652-3677.

Kumjian M R, Ryzhkov A V, Melnikov V M, et al. Rapid-scan super-resolution observations of a cyclic supercell with a dual-polarization WSR-88D[J]. Monthly weather review, 2010, 138(10): 3762-3786.

Liu D, Sun M, Su D, et al. A five-year climatological lightning characteristics of linear mesoscale convective systems over North China[J]. Atmospheric Research, 2021, 256: 105580.

Li X, Zhang Q, Xue H. The role of initial cloud condensation nuclei concentration in hail using the WRF NSSL 2-moment microphysics scheme[J]. Advances in Atmospheric Sciences, 2017, 34(9): 1106-1120.

Liu Z, Gao W, Yu Y, et al. Characteristics of PM 2.5 mass concentrations and chemical species in urban and background areas of China: emerging results from the CARE-

China network[J]. Atmospheric Chemistry and Physics, 2018, 18(12): 8849-8871.

Li Z, Wang Y, Guo J, et al. East asian study of tropospheric aerosols and their impact on regional clouds, precipitation, and climate (EAST - AIRCPC)[J]. Journal of Geophysical Research: Atmospheres, 2019, 124(23): 13026-13054.

Lynn B, Yair Y, Shpund J, et al. Using Factor Separation to Elucidate the Respective Contributions of Desert Dust and Urban Pollution to the 4 January 2020 Tel Aviv Lightning and Flash Flood Disaster[J]. Journal of Geophysical Research: Atmospheres, 2020, 125(24): e2020JD033520.

Lynn B, Khain A, Rosenfeld D, et al. Effects of aerosols on precipitation from orographic clouds[J]. Journal of Geophysical Research: Atmospheres, 2007, 112(D10).

MacGorman D R, Rust W D, Schuur T J, et al. TELEX the thunderstorm electrification and lightning experiment[J]. Bulletin of the American Meteorological Society, 2008, 89(7): 997-1014.

Mansell E R, Ziegler C L. Aerosol effects on simulated storm electrification and precipitation in a two-moment bulk microphysics model[J]. Journal of the Atmospheric Sciences, 2013, 70(7): 2032-2050.

Mansell E R, Ziegler C L, Bruning E C. Simulated electrification of a small thunderstorm with two-moment bulk microphysics[J]. Journal of the Atmospheric Sciences, 2010, 67(1): 171-194.

Mansell E R, MacGorman D R, Ziegler C L, et al. Charge structure and lightning sensitivity in a simulated multicell thunderstorm[J]. Journal of Geophysical Research: Atmospheres, 2005, 110(D12).

Mitzeva R, Latham J, Petrova S. A comparative modeling study of the early electrical development of maritime and continental thunderstorms[J]. Atmospheric research, 2006, 82(1-2): 26-36.

Mlawer E J, Taubman S J, Brown P D, et al. Radiative transfer for inhomogeneous atmospheres: RRTM, a validated correlated - k model for the longwave[J]. Journal of Geophysical Research: Atmospheres, 1997, 102(D14): 16663-16682.

Naccarato K P, Pinto Jr O, Pinto I. Evidence of thermal and aerosol effects on the cloud-

to-ground lightning density and polarity over large urban areas of Southeastern Brazil[J]. Geophysical Research Letters, 2003, 30(13).

Orville R E, Huffines G, Nielsen‐Gammon J, et al. Enhancement of cloud-to-ground lightning over Houston, Texas[J]. Geophysical Research Letters, 2001, 28(13): 2597-2600.

Price C. Global surface temperatures and the atmospheric electrical circuit[J]. Geophysical Research Letters, 1993, 20(13): 1363-1366.

Price C, Rind D. A simple lightning parameterization for calculating global lightning distributions[J]. Journal of Geophysical Research Atmospheres, 1992, 97(D9):9919-9933.

Qie K, Qie X, Tian W. Increasing trend of lightning activity in the South Asia region[J]. Science Bulletin, 2021, 66(1): 78-84.

Qie X, Yuan S, Chen Z, et al. Understanding the dynamical-microphysical-electrical processes associated with severe thunderstorms over the Beijing metropolitan region[J]. Science China Earth Sciences, 2020: 1-17.

Qie X, Yuan T, Xie Y, et al. Spatial and temporal distribution of lightning activities on the Tibetan Plateau[J]. Chinese Journal of Geophysics, 2004, 47(6): 1122-1127.

Reynolds S E, Brook M, Gourley M F. Thunderstorm charge separation[J]. Journal of Meteorology, 1957, 14(5): 426-436.

Rosenfeld D, Lohmann U, Raga G B, et al. 2008. Flood or drought: How do aerosols affect precipitation?[J]. Science, 321(5894): 1309-1313.

Rosenfeld D, Woodley W L. 2000. Deep convective clouds with sustained supercooled liquid water down to -37.5 ℃[J]. Nature, 405(6785): 440.

Saunders C P R, Peck S L, Varela G G A, et al. A laboratory study of the influence of water vapour and mixing on the charge transfer process during collisions between ice crystals and graupel[J]. Atmospheric Research, 2001, 58(3):187-203.

Saunders C P R, Peck S L. Laboratory studies of the influence of the rime accretion rate on charge transfer during crystal/graupel collisions[J]. Journal of Geophysical Research: Atmospheres, 1998, 103(D12): 13949-13956.

Saunders C P R, Keith W D, Mitzeva R P. The effect of liquid water on thunderstorm

charging[J]. Journal of Geophysical Research: Atmospheres, 1991, 96(D6): 11007-11017.

Simpson G C, Scrase F J. The distribution of electricity in thunderclouds[J]. Proceedings of the Royal Society of London. Series A-Mathematical and Physical Sciences, 1937, 161(906): 309-352.

Srivastava A, Tian Y, Qie X S, et al. 2017. Performance assessment of Beijing Lightning Network (BLNET) and comparison with other lightning location networks across Beijing. Atmospheric Research, 197 76-83.

Stolz D C, Rutledge S A, Pierce J R. Simultaneous influences of thermodynamics and aerosols on deep convection and lightning in the tropics[J]. Journal of Geophysical Research: Atmospheres, 2015, 120(12): 6207-6231.

Storer R L, Van Den Heever S C, Stephens G L. Modeling aerosol impacts on convective storms in different environments[J]. Journal of the Atmospheric Sciences, 2010, 67(12): 3904-3915.

Sun M, Qie X, Liu D, et al. Analysis of potential effects of aerosol on lightning activity in Beijing metropolitan region[J]. Chinese Journal of Geophysics, 2020, 63(5): 1766-1774.

Takahashi T. A numerical simulation of winter cumulus electrification. Part I: Shallow cloud[J]. Journal of the Atmospheric Sciences, 1983, 40(5): 1257-1280.

Takahashi T. Riming electrification as a charge generation mechanism in thunderstorms[J]. Journal of the Atmospheric Sciences, 1978, 35(8): 1536-1548.

Tan Y B, Ma X, Xiang C Y, et al. A numerical study of the effects of aerosol on electrification and lightning discharges during thunderstorms[J]. Chinese Journal of Geophysics, 2017, 60(8): 3041-3050.

Tao W K, Chen J P, Li Z, et al. Impact of aerosols on convective clouds and precipitation[J]. Reviews of Geophysics, 2012, 50(2).

Thomas R J, Krehbiel P R, Rison W, et al. Observations of VHF source powers radiated by lightning[J]. Geophysical Research Letters, 2001, 28(1): 143-146.

Thornton J A, Virts K S, Holzworth R H, et al. 2017. Lightning enhancement over major oceanic shipping lanes[J]. Geophysical Research Letters, 44(17).

Twomey, S., 1959: The nuclei of natural cloud formation, Part II: The supersaturation in natural clouds and the variation of cloud droplet concentration. Geofis. Pura Appl., 43, 243–249.

Van Den Broeke M S, Straka J M, Rasmussen E N. Polarimetric radar observations at low levels during tornado life cycles in a small sample of classic southern plains supercells[J]. Journal of applied meteorology and climatology, 2008, 47(4): 1232-1247.

Wang Q, Li Z, Guo J, et al. 2018. The climate impact of aerosols on the lightning flash rate: is it detectable from long-term measurements?[J]. Atmospheric Chemistry and Physics, 18(17).

Wang Y, Qie X S, Wang D F, et al. 2016. Beijing Lightning Network (BLNET) and the observation on preliminary breakdown processes [J]. Atmos. Res., 171: 121–132.

Wang Y, Wan Q, Meng W, et al. Long-term impacts of aerosols on precipitation and lightning over the Pearl River Delta megacity area in China[J]. Atmospheric Chemistry and Physics, 2011, 11(23): 12421-12436.

Westcott N E. Summertime cloud-to-ground lightning activity around major Midwestern urban areas[J]. Journal of Applied Meteorology, 1995, 34(7): 1633-1642.

Williams E, Mushtak V, Rosenfeld D, et al. Thermodynamic conditions favorable to superlative thunderstorm updraft, mixed phase microphysics and lightning flash rate[J]. Atmospheric Research, 2005, 76(1-4): 288-306.

Williams E, Stanfill S. The physical origin of the land–ocean contrast in lightning activity[J]. Comptes Rendus Physique, 2002, 3(10): 1277-1292.

Williams E. The tripole structure of thunderstorms[J]. Journal of Geophysical Research, 1989: 13151-13167.

Xiong Y J, Qie X S, Zhou Y J, et al. Regional responses of lightning activities to relative humidity of the surface[J]. Chinese Journal of Geophysics, 2006, 49(2): 311-318.

Yair Y, Lynn B, Yaffe M, et al. Observations and numerical simulations of the October 25th, 2015 super-cell thunderstorm over Central Israel[J]. Atmospheric Research, 2021, 247: 105165.

Yair Y. Lightning hazards to human societies in a changing climate[J]. Environmental Research Letters, 2018, 13(12).

Yair Y, Lynn B, Price C, et al. Predicting the potential for lightning activity in Mediterranean storms based on the Weather Research and Forecasting (WRF) model dynamic and microphysical fields[J]. Journal of Geophysical Research, 2010.

Yair Y. Charge generation and separation processes[J]. Space Science Reviews, 2008, 137(1-4): 119-131.

Yuan T, Remer L A, Pickering K E, et al. Observational evidence of aerosol enhancement of lightning activity and convective invigoration[J]. Geophysical Research Letters, 2011, 38(4).

Zhang R, Jing J, Tao J, et al. Chemical characterization and source apportionment of PM 2.5 in Beijing: seasonal perspective[J]. Atmospheric Chemistry and Physics, 2013, 13(14): 7053-7074.

Zhao P, Li Z, Xiao H, et al. Distinct aerosol effects on cloud-to-ground lightning in the plateau and basin regions of Sichuan, Southwest China[J]. Atmospheric Chemistry and Physics, 2020, 20(21): 13379-13397.

Zhao P, Yin Y, Xiao H. The effects of aerosol on development of thunderstorm electrification: A numerical study[J]. Atmospheric Research, 2015, 153: 376-391.

Ziegler C L, MacGorman D R. Observed lightning morphology relative to modeled space charge and electric field distributions in a tornadic storm[J]. Journal of Atmospheric Sciences, 1994, 51(6): 833-851.

Ziegler C L, MacGorman D R, Dye J E, et al. A model evaluation of noninductive graupel‐ice charging in the early electrification of a mountain thunderstorm[J]. Journal of Geophysical Research: Atmospheres, 1991, 96(D7): 12833-12855.

Ziegler C L. Retrieval of thermal and microphysical variables in observed convective storms. Part 1: Model development and preliminary testing[J]. Journal of the Atmospheric Sciences, 1985, 42(14): 1487-1509.

Table 1. Settings for the nested simulations

Model Option	Outer D01	Inner D02
Domain Coverage	6 km, 442×391	2 km, 496×496
Vertical levels	40	40
Time step	30 s	10 s
Microphysics Scheme	NSSL two-moment	NSSL two-moment
Longwave Radiation	RRTM	RRTM
Shortwave Radiation	Dudhia	Dudhia
Boundary Layer	BouLac PBL	BouLac PBL
Land Surface	Unified Noah LSM	Unified Noah LSM

Table 2. Temporal evolution of the thunderstorm.

	Observation (UTC)	Simulations (UTC)	
		C-case	P-case
Formation	10:48	09:18	09:18
Beginning stage	10:48-11:30	09:18-09:30	09:18-10:00
Developing stage	11:30-12:30	09:30-10:30	10:00-11:00
Mature stage	12:30-13:30	10:30-12:00	11:00-12:36
Dissipating stage	13:30-18:06	12:00-15:36	12:36-16:36

Table 3. Domain-averaged Properties of Hydrometeors.

	Number Concentration (10^3 kg^{-1})		Mean-mass Radius (μm)	
	C-case	**P-case**	**C-case**	**P-case**
Cloud droplets	3930	7910	6.5	6.1
Rain drops	0.069	0.031	154.1	179.9
Ice Crystals	2280	3850	3235.8	2994.9
Graupel	0.028	0.012	322.4	479.5

Table 4. Comparison of Convective Properties.

765

	C-case	**P-case**
Time	10:36 UTC	10:48 UTC
Height	10.5 km	12.5 km
Maximum velocity	50.4 m/s	53.5 m/s
Cloud top height	15 km	15 km
Cloud base height	0.5 km	0.5 km

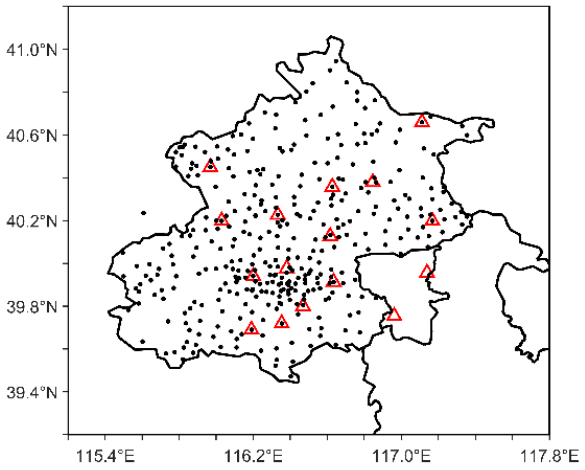

770 **Figure 1** Spatial distributions of BLNET stations (red triangles), and ground-based automatic weather stations (black dots) in the Beijing region.

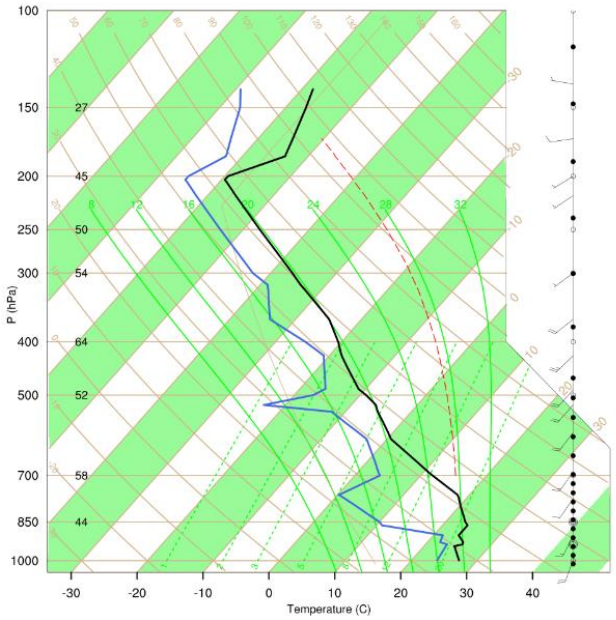

Figure 2 Sounding profiles for Beijing at 00:00 UTC on Aug11, 2017. The black, blue solid lines and red dashed line represent temperature, dew point, parcel adiabatic lapse rate, respectively.

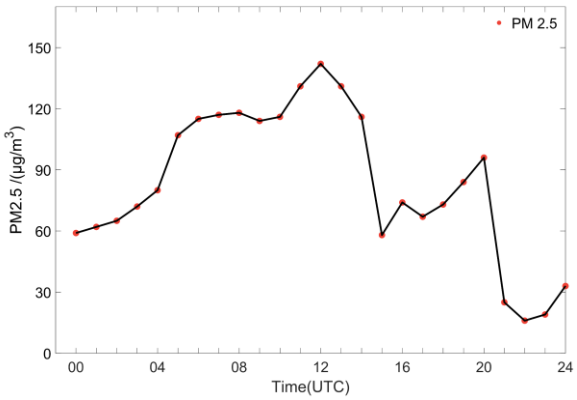

Figure 3 Hourly mass concentration of $PM_{2.5}$ on Aug11, 2017 at Beijing urban area.

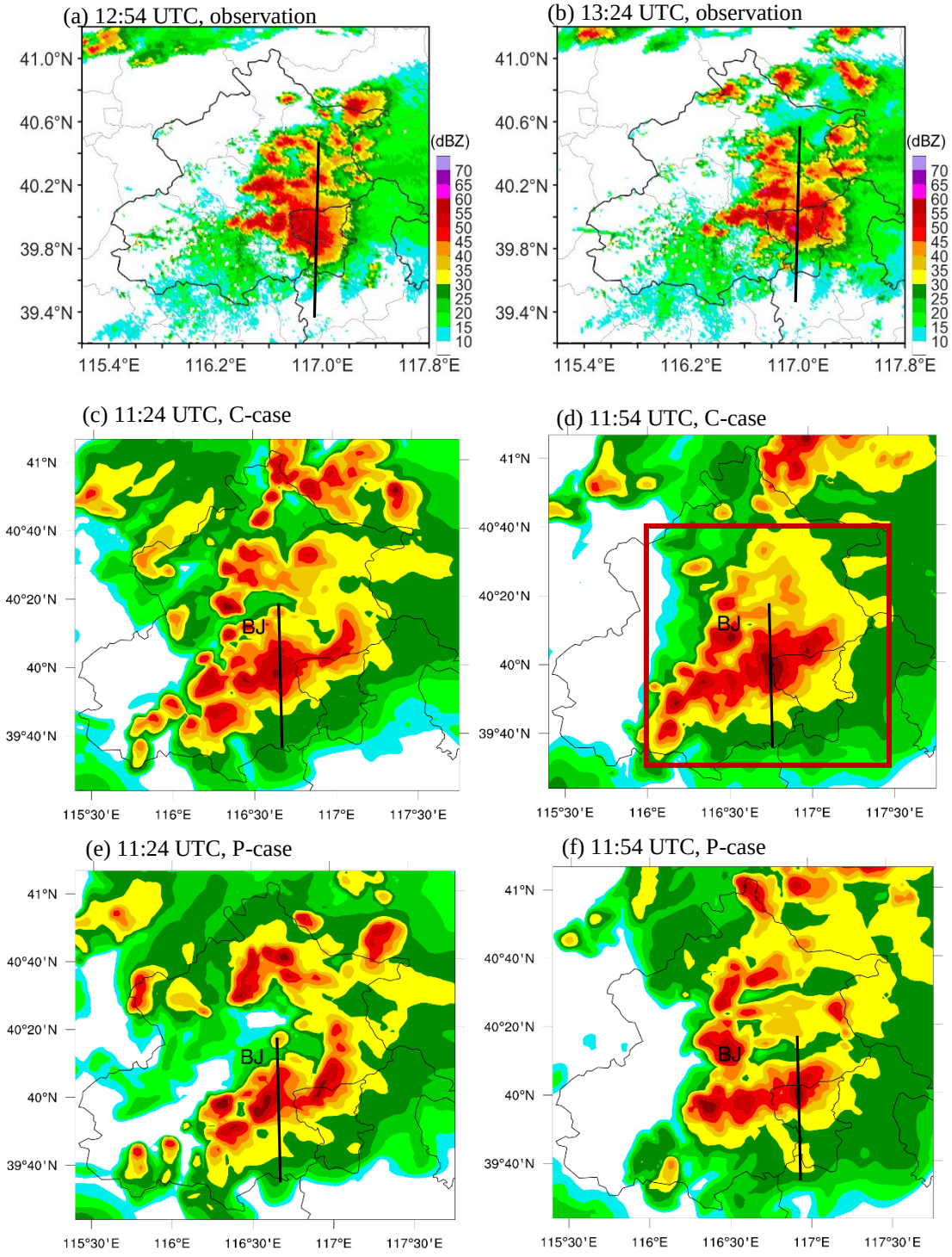

785 **Figure 4** Radar reflectivity (unit: dBZ) between observation and simulation for the C- and P-cases, the simulation was earlier than observation about 1.5 h. (a)-(b) Observation at 12:54 UTC and 13:24 UTC. (c)-(d) Simulation for the C-case at 11:24 UTC and 11:54 UTC. (e)-(f) Simulation for the P-case at 11:24 UTC and 11:54 UTC, respectively. The red rectangle in Fig. 4d denotes the region where the simulated results are analyzed in this study.

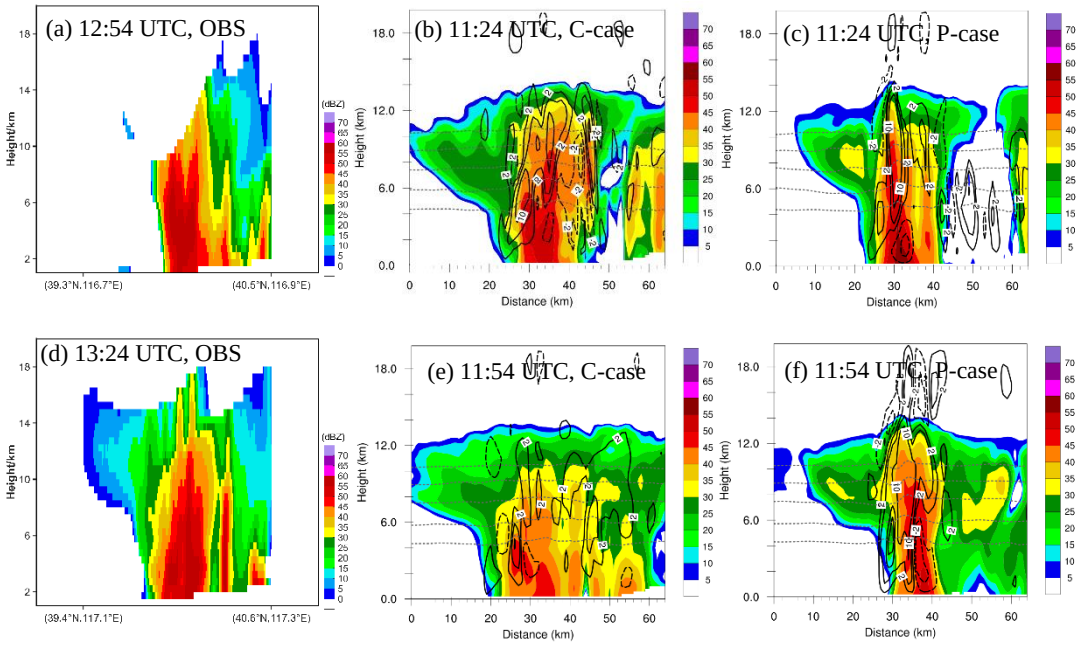

Figure 5 Comparison of vertical cross-section of radar reflectivity along the black line shown in Figure 4a-4f between observation and simulations. (a) Observation (black line shown in Fig.4a), (b) C-case (black line in Fig. 4c), (c) P-case (black line in Fig. 4e), (d) Observation (black line shown in Fig. 4b). (e) C-case (black line in Fig. 4d), and (f) P-case (black line in Fig. 4f).

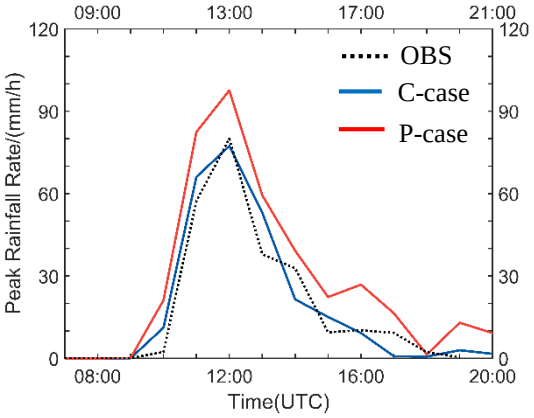

Figure 6 Temporal evolution of the peak rainfall rate for observation and simulations. The black dashed line represents the observation, the red line corresponds to the P-case, and the blue line corresponds to the C-case. The x-axis above is for the observation, the x-axis below is for the simulations.

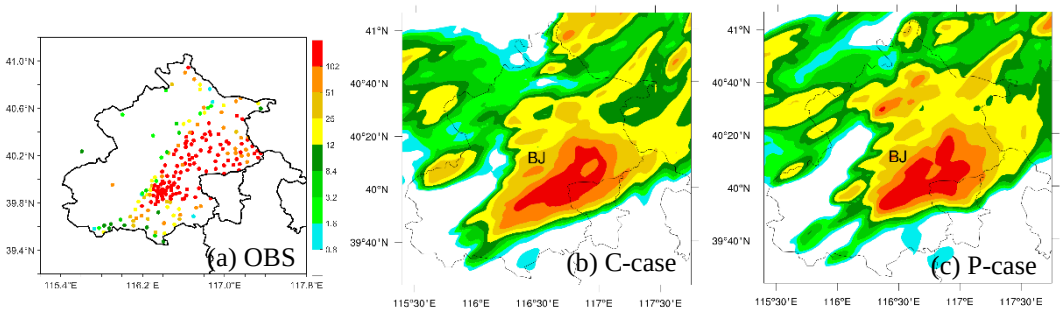

Figure 7 Comparison of accumulated precipitation (units: mm) between observation (11:00-17:00 UTC) and simulations (10:00-16:00 UTC). (a) Observation. (b) C-case, and (c) P-case.

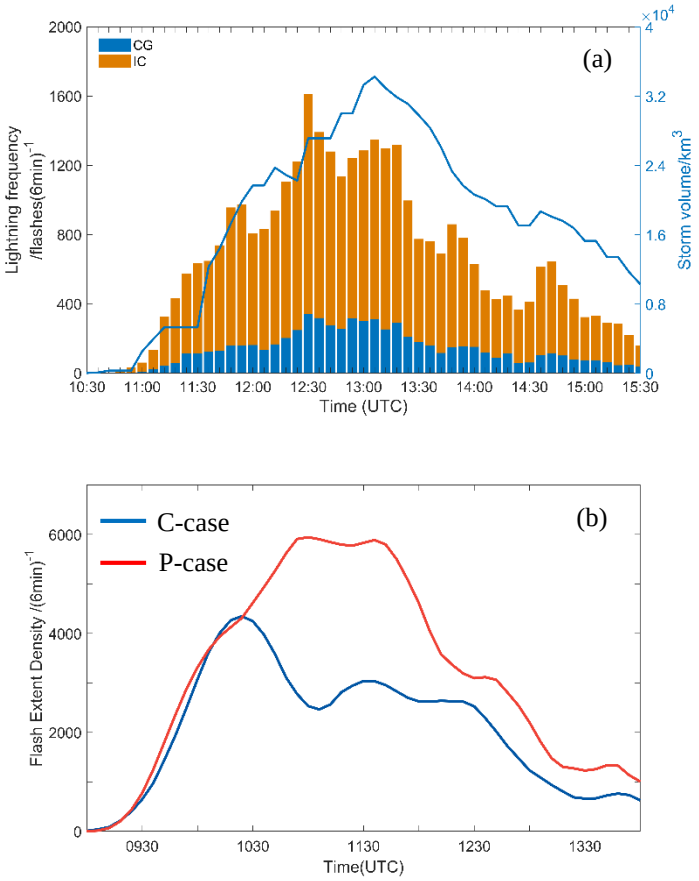

Figure 8 Temporal variation in (a) observed total lightning frequency and (b) simulated flash extent density (FED). In (a), orange represents IC lightning and blue represents CG lightning. The solid line represents the storm volume associated with radar reflectivity exceeding 30 dBZ. In (b), red line represents the P-case and blue line represents the C-case.

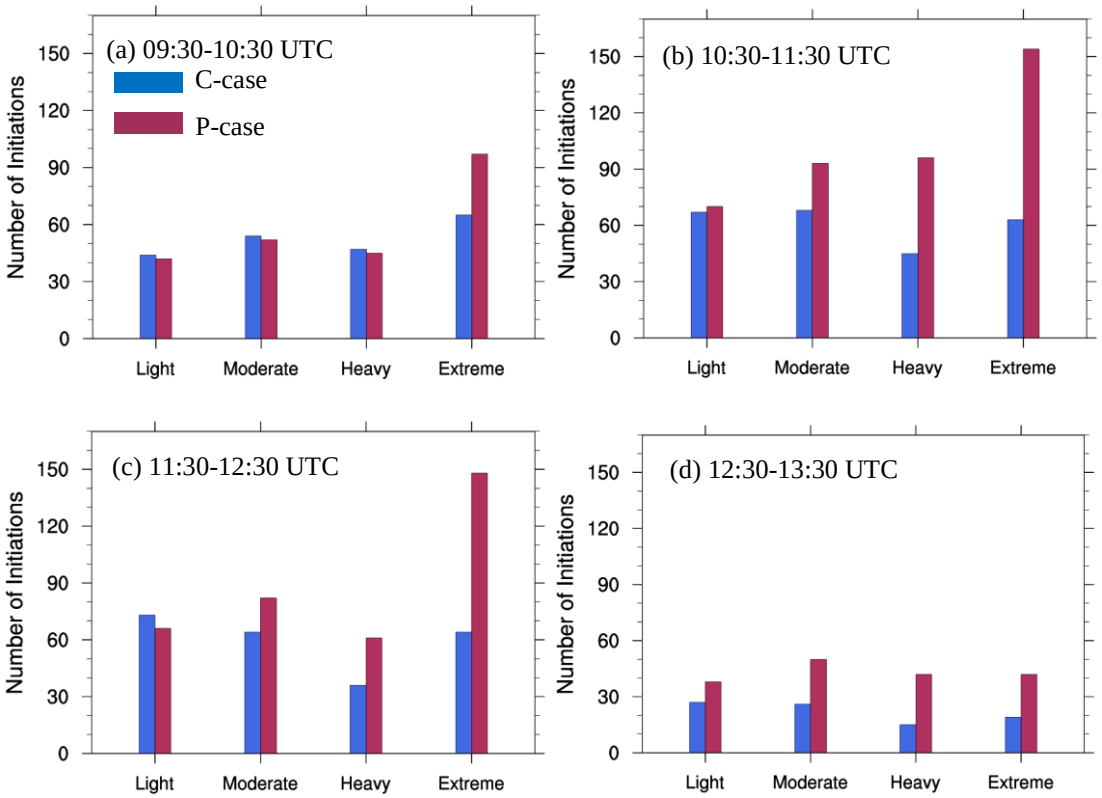

Figure 9 Number of initiations for different lightning intensity categories in different time, i.e. light (50-100 grid points), moderate (100-200 grid points), heavy (200-300 grid points) and extreme (>300 grid points), simulated for the P- and C-cases.

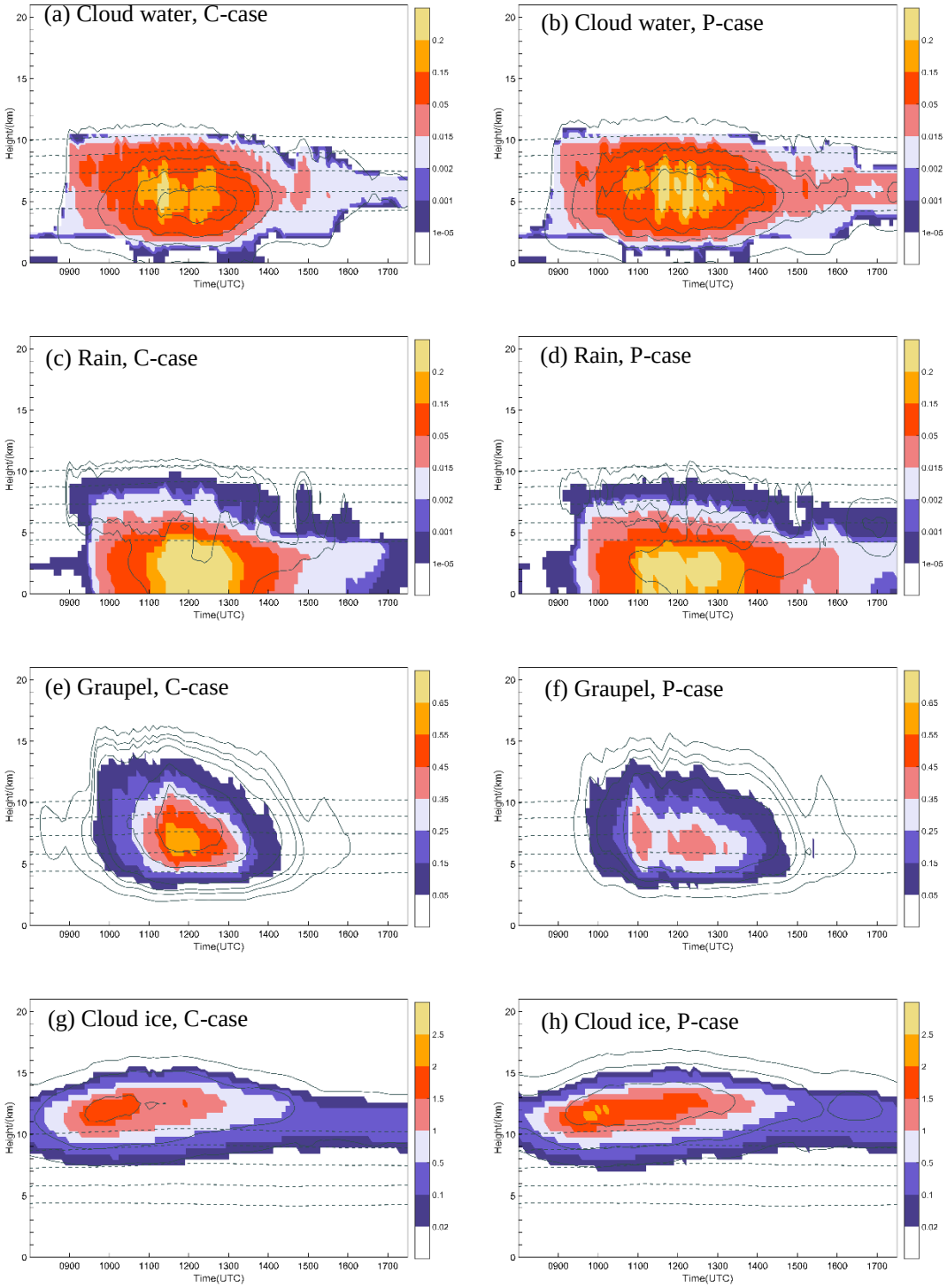

825

(figure continued on next page)

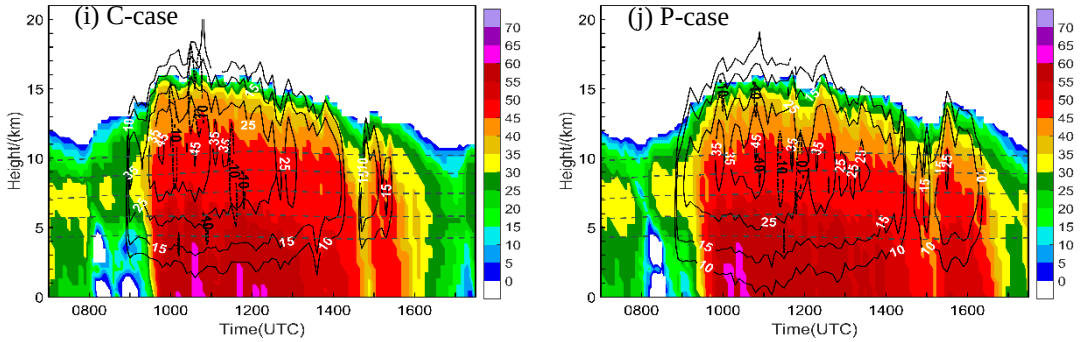

Figure 10 (a)-(h) Temporal variation of the vertical profiles of domain-averaged mass mixing ratio (g kg^{-1}, shaded) and number concentration (kg^{-1}, solid lines) of (a) cloud water in the C-case, (b) cloud water in P-case, (c) rain water in the C-case, (d) rain water in the P-case, (e) graupel in the C-case, (f) graupel in the P-case, (g) ice in the C-case, (h) ice in the P-case. Contour levels in (a)-(h) for cloud water number concentration are 10^6, 2×10^7, 5×10^7, 10^8 kg^{-1}, and for rain water are 100, 300 kg^{-1}, and for graupel are 10, 30, 50, 100, 300, 500, 700, 1000 kg^{-1}, and for ice are 0.1×10^7, 1×10^7, 5×10^7 kg^{-1}. (i)-(j) Time-height maximum simulated radar reflectivity (color shading, unit: dBZ) and maximum vertical velocities (solid line and white label: 10, 15, 25, 35, 45 m s^{-1}; dashed line and black label: -10, -15 m s^{-1}) for (i) the C-case and (j) the P-case. The 0 ℃, -10 ℃, -20 ℃, -30 ℃ and -40 ℃ isotherms are shown by the dashed gray lines in (a)-(j).

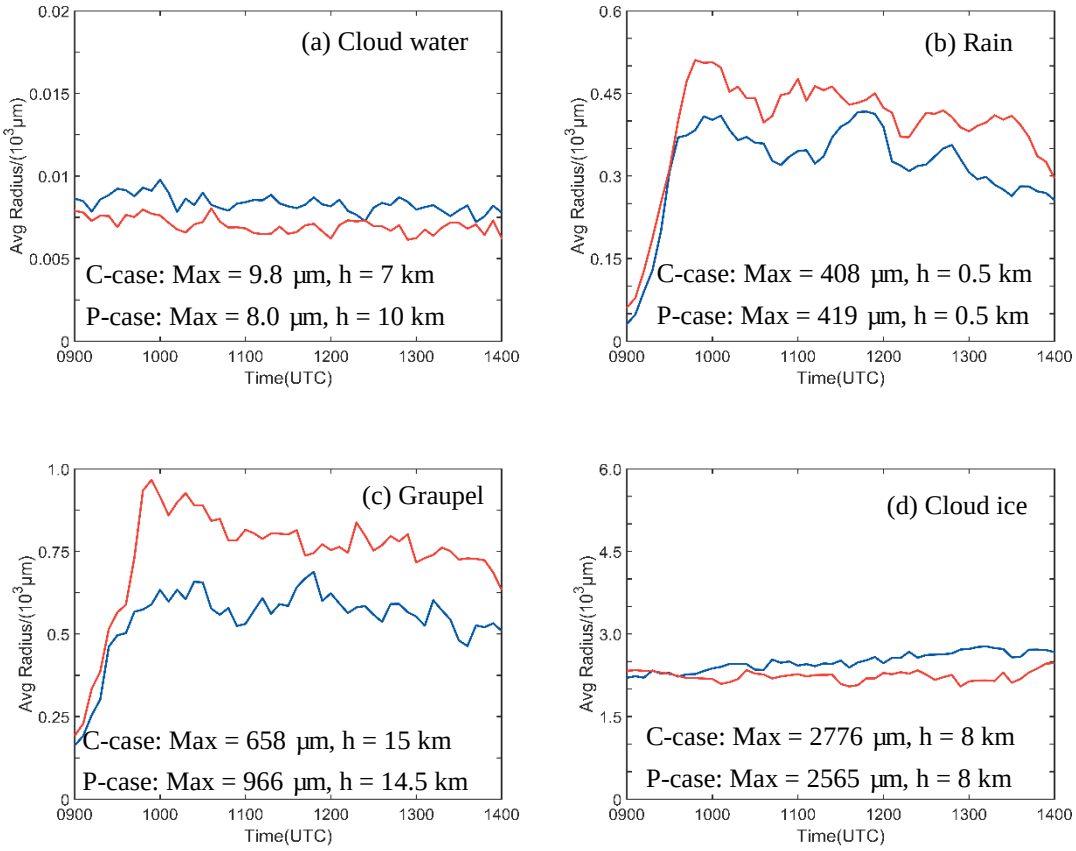

Figure 11 Temporal variation of domain-averaged effective radius for the different hydrometeors. (a) cloud water, (b) rainwater, (c) graupel, (d) ice. The red lines represent the P-case and the blue lines represent the C-case.

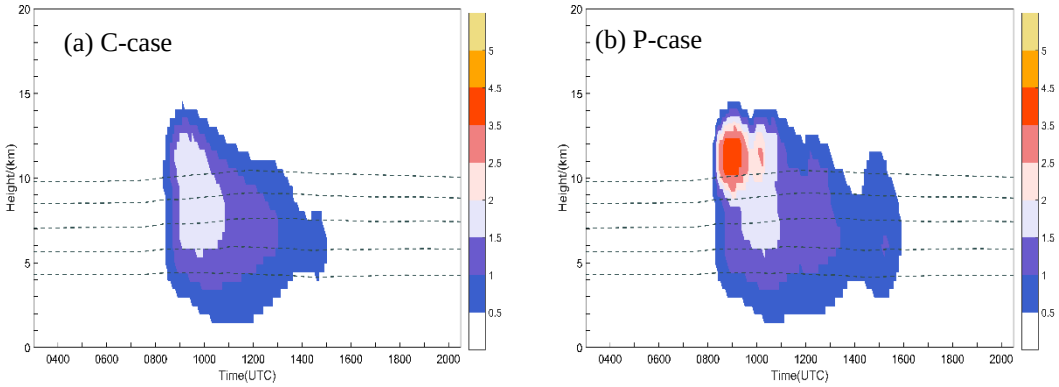

Figure 12 Temporal variation of the vertical profiles of peak latent heating (K hour^{-1}, shaded) of (a) C-case, and (b) P-case. The 0 ℃, -10 ℃, -20 ℃, -30 ℃ and -40 ℃ isotherms are shown by the dashed gray lines in (a)-(b).

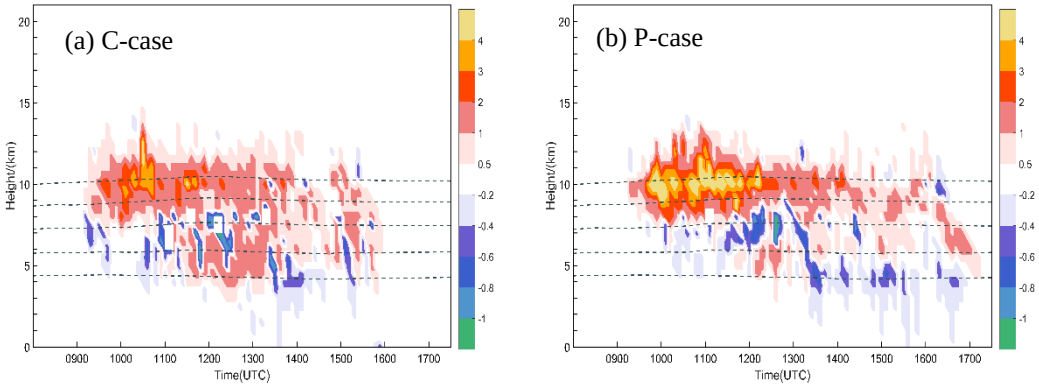

Figure 13 Temporal variation of the vertical profiles of peak positive (negative) charge density (nC m^{-3}, shaded) of (a) C-case, and (b) P-case. The 0 ℃, -10 ℃, -20 ℃, -30 ℃ and -40 ℃ isotherms are shown by the dashed gray lines in (a)-(b).

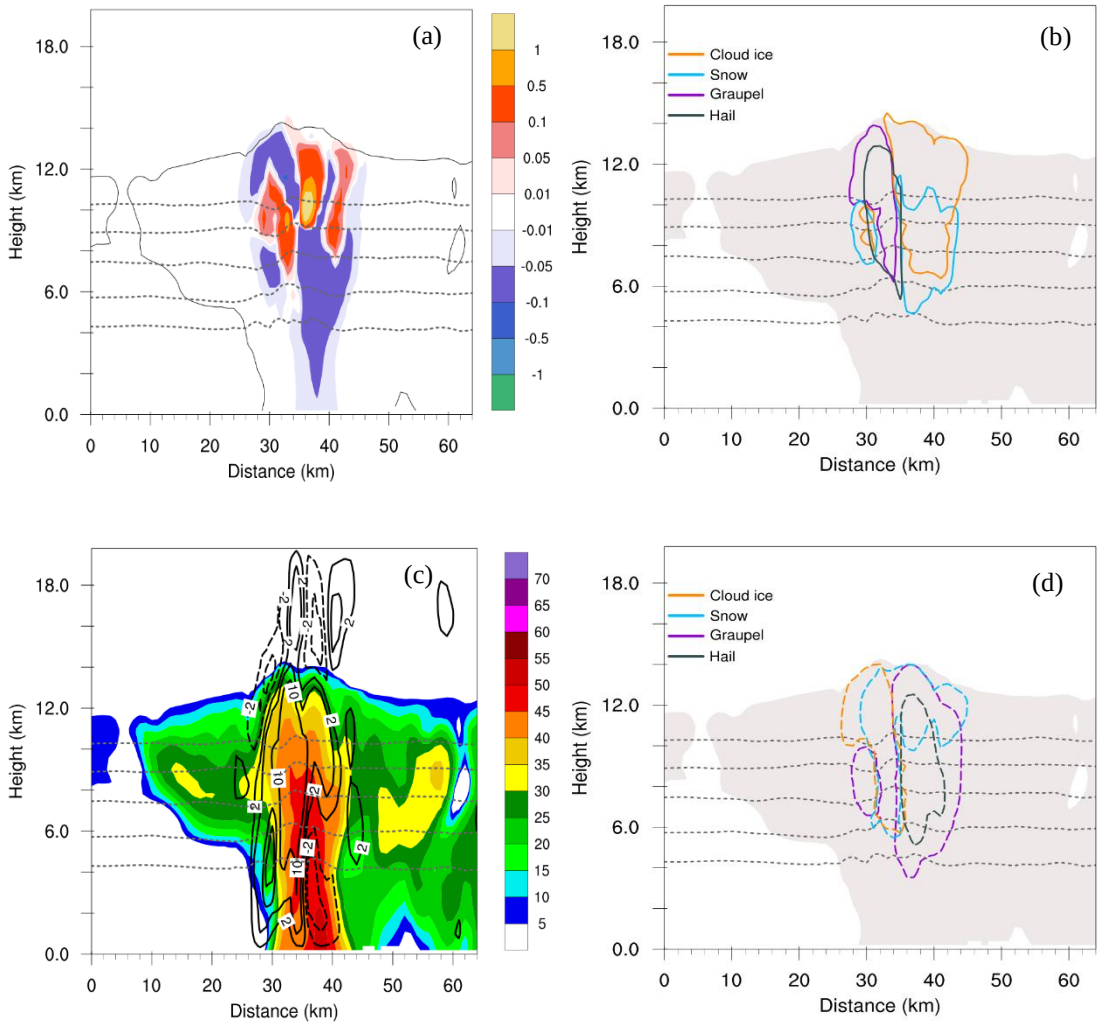

Figure 14 Vertical cross sections (south to north) at the location shown in Fig. 4f of simulated variables at the mature stage of the thunderstorm (11:54 UTC) in the P-case. (a) Total net space charge (nC m^{-3}, shaded). The 0 ℃, -10 ℃, -20 ℃, -30 ℃ and -40 ℃ isotherms are shown by dashed gray lines in (a)-(d). (b) +0.1 nC m^{-3} space charge density contours for cloud ice (orange), snow (blue), graupel (purple), and hail (black). The cloud outline (reflectivity echoes ≥ 5 dBZ) is denoted by the gray shaded contour. (c) Radar reflectivity (unit: dBZ), black lines for vertical velocities (solid line: 2, 5, 10 m s^{-1}; dashed line: -2 m s^{-1}). (d) As in (b), but for -0.1 nC m^{-3} charge density.

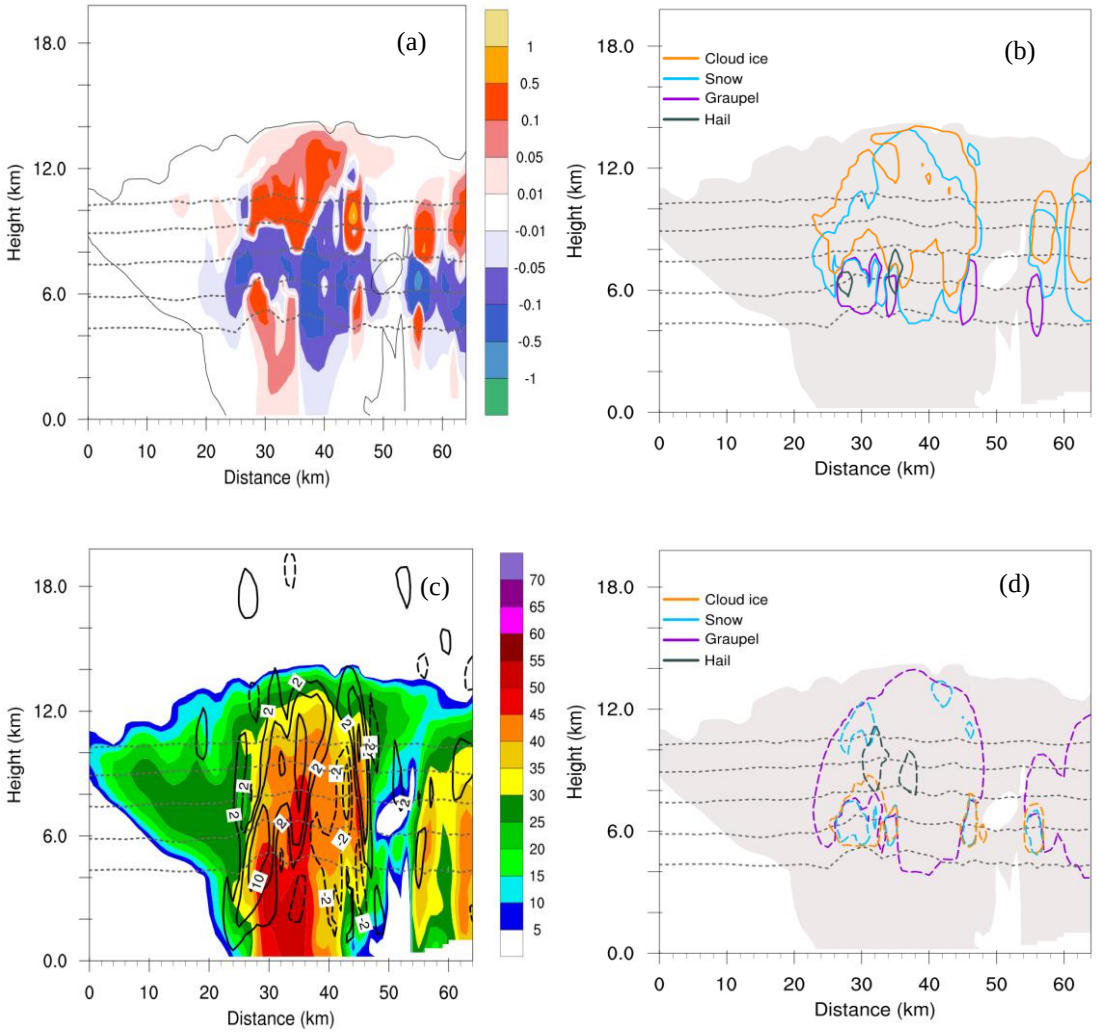

Figure 15 As in Fig. 14, but the vertical cross sections at the location shown in Fig. 4c of simulated variables at the mature stage of the thunderstorm (11:24 UTC) in the C-case.

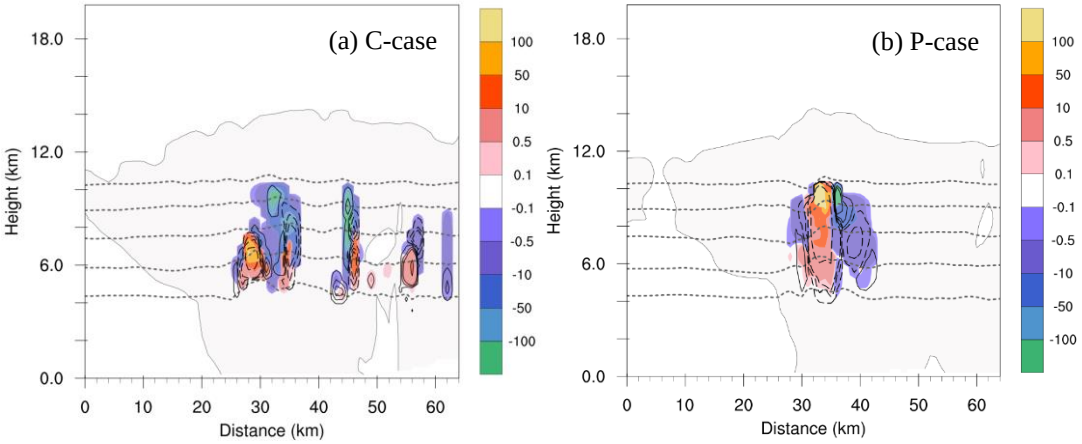

Figure 16 Vertical cross sections (south to north) at the locations shown in Fig. 4c and 4f of non-inductive (pC m^{-3} s^{-1}, shaded) and inductive (solid lines: 0.1, 0.5, 1 pC m^{-3} s^{-1}; dashed lines: -0.1, -0.5, -1, -5, -10 pC m^{-3} s^{-1}) charging rates at the mature stage of (a) C-case (11:24 UTC, Fig. 4c), and (b) P-case (11:54 UTC, Fig. 4f). The 0 ℃, -10 ℃, -20 ℃, -30 ℃ and -40 ℃ isotherms are shown by dashed gray lines.

880

Interactive comment on "Aerosol Effects on Electrification and Lightning Discharges in a Multicell Thunderstorm Simulated by the WRF-ELEC Model" by Mengyu Sun et al.

M. Sun et al.

sunmengyu16@mails.ucas.edu.cn

Reply to Referee 1

This work uses an advanced microphysical scheme coupled with a charging and discharge model to study the effect of pollution on microphysical and charging processes. The subject is of interest to readers of the Journal.

Yet, there is much work to be done to clarify the reasons for the differences between the continental and polluted case. I am also concerned that the results are not realistic in regard to how the cloud and rain water forms as the background conditions are changed. The authors offer explanations for why they do not, but they contradict themselves within the text.

I highlighted areas of text that were not grammatically correct or were unclear (in attachment). I also listed my comments here that are mentioned within bubbles in the attached text. Words are used describing results that require further explanation (e.g., what is a domain average? The authors stated that they did not use some of their results because they were not realistic). There is a lack of quantitative comparison. There are many highlighted areas and many comments.

I suggest the authors step back and ask themselves if the microphysical response to changes in aerosol concentration are consistent with other studies, including spectral (bin) microphysics studies, as well as observation!

They need to more clearly explain model simulation differences and add details where needed (see comments).

I do not see why Section 4.5 (Delay of First Flash) is its own section, coming well after the previous results that followed the storms through their different developmental

phases.

Response:

We appreciate these valuable comments. We have studied them carefully and have addressed them in the revised manuscript. Below are the point-by-point responses to the reviewer's comments.

120: No reference provided.

Response:

Thanks. We added citations as suggested: "**The special terrain condition with mountain in the northwest and ocean in the southeast (Qie et al., 2020), as well as heat island effect and elevated aerosol loading in the urban region (Zhang et al., 2013; Liu et al., 2018)…**" (Revised version, lines 122-125)

125: What is the context for stating "The maximum total lightning frequency even exceeded 1600 flashes $(6\ \text{min})^{-1}$ at the mature stage." How does the reader know this is a large number, considering system sensitivity varies from region to region.

Response:

Thanks for the reminder. We have revised the context to explain the intensity of this lightning activity and added references: "**The total lightning flashes of this case accounted for one-third of the total number of lightning flashes during the 2017 warm season (Chen et al., 2020).**" (Revised version, lines 129-130)

130: Where is the description of the model physics used, the domain grid spacing, etc?

How long were the simulations run? How soon after the start of the simulations did the convection of interest occur?

Response:

Thanks for the comments. We have added the description of the model physics used in this study, as well as the related information of the simulations. (Revised version, lines 207-220)

135: Why are processes related to graupel growth the only ones mentioned? I was expecting to read more details about diffusional growth, interactions among particles, freezing, etc.

Response:

Thanks. We only previously mentioned graupel growth because that the predicted graupel density is variable. And that makes it possible for the single graupel category to represent a range of particles from high-density frozen drops to low-density graupel (Mansell et al., 2010). We have added more details of the two-moment bulk microphysics scheme. (Revised version, lines 137-149)

170: higher in the Beijing area than where else?

Response:

Thanks for this comment. We have added the hourly average mass concentration of $PM_{2.5}$ on 11 August 2017, and added related reference as follows: "**The hourly-average value of the observed $PM_{2.5}$ concentration before the thunderstorm initiation (more than 110 μg m^{-3}) is much higher than the 3-year mean $PM_{2.5}$ concentration (69.4±54.8 μg m^{-3}) in the Beijing area (Liu et al., 2018).**" (Revised version, lines 224-227, Figure 3)

180: should be: "should effectively delay..." There is no certainty here.

Response:

We agree to this suggestion and have corrected in the revised manuscript.

185: There are quite large differences in the simulated radar compared to the observed radar in terms of spatial coverage. The authors should say why, and explain why these large differences do not affect their results/conclusions. Also, can the authors hypothesize why the simulated stormed occurred 1.5 earlier than observed? This is quite a significant time difference.

Response:

These are good questions and comments. These comments contain 2 questions. We'll deal with them one by one.

(A) Regarding the differences in the simulated radar compared to the observation.

In order to explain these difference do not affect our results, we have made comparison of the radar reflectivity as a function of time, hourly peak rainfall rate, and the spatial distribution of precipitation between the observation and both simulations (revised version, Figure 5, 6, and 7). The comparisons show that the simulated distributions and spatio-temporal development of radar reflectivity and precipitation under polluted condition are in overall agreement with observations. In additional, we added related analysis in Part "**4.1 Radar reflectivity, precipitation and lightning flashes of multicell**" (revised version, lines 246-250; lines 255-273). With such information, the analysis of the physical processes is much appropriate for explaining the difference in the electrification and discharging in both simulated cases.

(B) Regarding why the simulated storm occurred 1.5 h earlier than the observation.

In our study, we use 3-hourly NCEP GFS data with resolution of 0.5 °×0.5 °and the WRF Processing System (WPS) to configure real-time simulations. The nesting

technique from a domain with a resolution of 50 km×50 km to a domain with a resolution of 6 km ×6 km probably brings about instability of the simulations. Data assimilation was not applied to nudge the synoptic pattern toward the Global Forecast System (GFS) data. While assimilation of observational data can effectively improve the high-impact weather forecasting (Sun et al., 2014; Gustafssn et al., 2018). And the simulations began at 00:00 UTC on 11 August 2017, while the simulated thunderstorm formed at 09:18 UTC, which means the spin-up of the background aerosol is a little short (Lynn et al., 2020). These reasons probably result in the simulated stormed occurred 1.5 h earlier than observed. As mentioned above, we have made comparisons of radar reflectivity and precipitation, and the results show that the simulated distributions and spatio-temporal development of radar reflectivity and precipitation under polluted condition are in overall agreement with observations. These comparisons mean that the analysis of the physical processes is appropriate for explaining the difference in the electrification and discharging in both simulated cases. And we would improve our simulations in the future accordingly.

205: How is the variation of flashed in the P-Case better (more) consistent with the observation. No statistics are presented to prove this point.

Response:

Thanks for the comment. We have used predicted flash extent density (FED), as well as grid points (grids where the simulated electric field exceeds a breakdown threshold) to assess the lightning activity between both simulations and the observation (revised version, lines 185-188; lines 201-204). In addition, we have presented related analysis in Part "**4.1 Radar reflectivity, precipitation and lightning flashes of multicell**". (Revised version, lines 282-290)

240: In previous simulation studies, the authors note that more aerosols could be activated into cloud drops ... leading to larger cloud drop concentration. They claim that in this study no more cloud droplets could be created -- suggesting that the supply of

moisture was limiting. However, this could be an artifact of the scheme, rather than physical reality. Moreover, in 255, the authors claim that warm rain process was delayed -- yet why should it be, since the cloud concentration (mass/) was just mentioned to be the same.

Response:

Thanks for the comment. This comment contain 2 questions. We'll deal with them one by one.

(A) Regarding the aerosols activated to cloud droplets.

In light of these comment, we have analyzed the radar reflectivity and precipitation (Figure 6, 7, revised version) at the beginning stage of the thunderstorm for the observation and both simulations. Since the observed radar reflectivity during 11:00-11:24 UTC is missing, so Figure R1 shows the radar echo before and after 11:15 UTC (09:45 UTC in simulations) for comparison. In the early stage of the thunderstorm, the radar echo for the P-case is relatively similar with these of the C-case. We realized that the area we chose in the initial stage was too small. The extra cell in figure 5j (initial version) probably because that the previous selected area did not include the cell in the C-case. Therefore, we have enlarged the region (shown in Figure 4d, revised version). The microphysics along with further electrification and lightning activities of this thunderstorm have been re-analyzed. With such improvements, we believe the analysis of the physical processes is much appropriate for explaining the difference in the electrification and discharging in both simulated cases. The results show that more aerosols could be activated into cloud droplets under polluted condition and more water vapor condenses onto these droplets. The related description has been modified in Part "**4.2 Microphysical properties of multicell"**. (Revised version, lines 323-360)

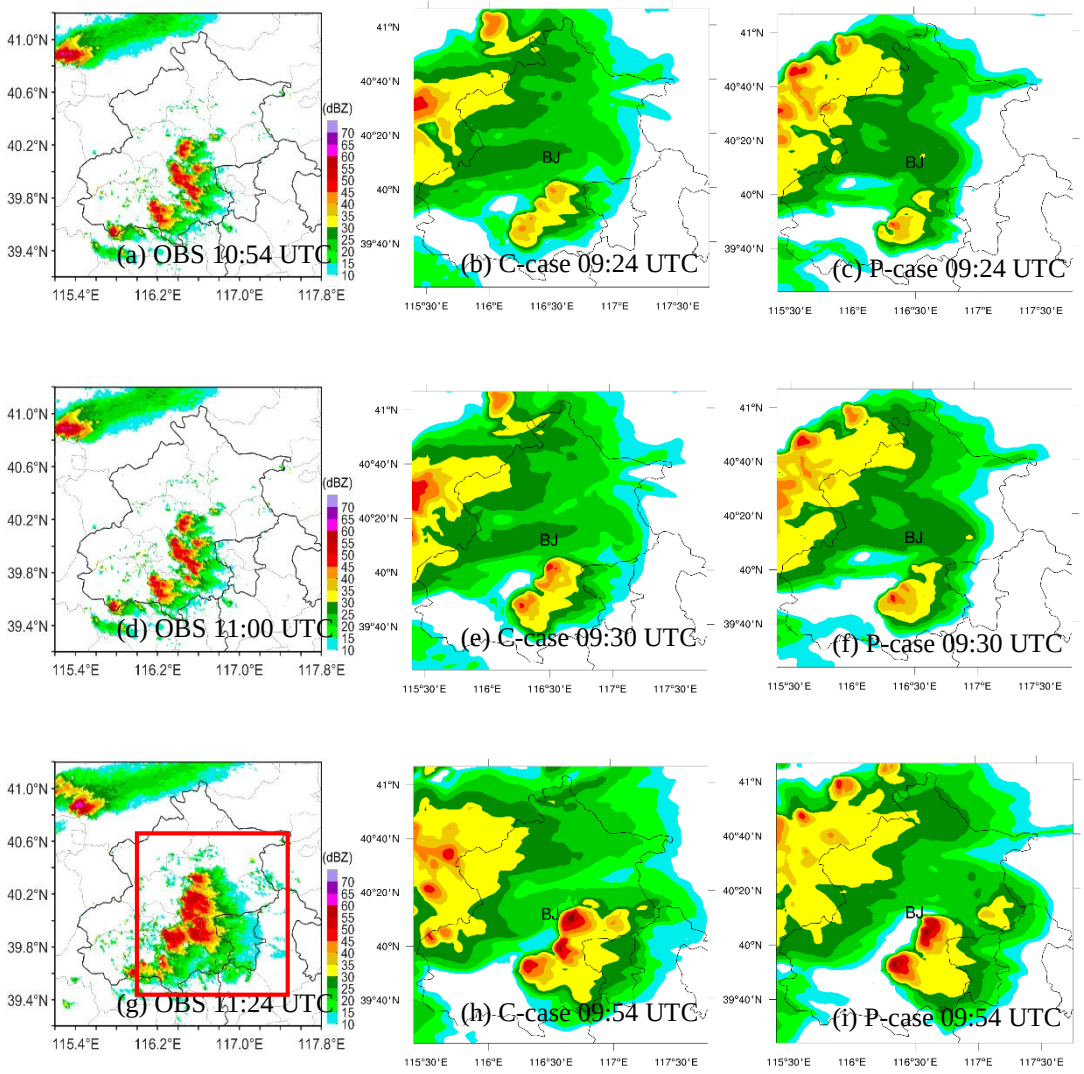

Figure R1 Radar reflectivity (unit: dBZ) between observation and simulation for the C- and P-cases, the simulation was earlier than observation about 1.5 h. (a), (d), (g) Observation at 10:54 UTC, 11:00 UTC and 11:24 UTC. (b), (e), (h) Simulation for the C-case at 09:24 UTC, 09:30 UTC and 09:54 UTC. (c), (f), (i) Simulation for the P-case at 09:24 UTC, 09:30 UTC and 09:54 UTC, respectively. The red rectangle in Fig. R2g denotes the region where the simulated results are analyzed in this study.

(B) Regarding the warm rain process.

We agree to the reviewer's comment. We have made the comparison of precipitation between the observation and both simulations (revised version, Figure 6, 7; lines 255-273), and found the warm rain processes was not delayed. We have deleted this sentence in the revised manuscript.

265: Moreover, latent heating profiles are similar in areas of cloud mass, again suggesting that warm processes were not delayed.

Response:

Thanks for the comment. Yes, the warm rain processes in this study were not delayed. And the temporal variation of the vertical profiles of peak latent heating has been added in Figure 12 (revised version) to make comparison of latent heat between both simulations during the whole duration of the thunderstorm. The latent heat shown in Figure 12 results from both condensation and freezing. In addition, related analysis has been added in Part "**4.2 Microphysical properties of multicell**". (Revised version, lines 327-329, 353-360)

260: Please add more up to date references.

Response:

Thanks for the suggestions and we have added related references as follows: "**Observations and simulations also found that the content of ice crystals could be greater under polluted condition, resulting from more condensation latent heat and strengthened updrafts (Khain et al., 2008; Koren et al., 2010; Wang et al., 2011; Zhao et al., 2015; Tan et al., 2017; Lynn et al., 2020).**" (Revised version, lines 341-344)

270: They state that the mass mixing ratio of graupel was relatively less in the P-case. This is contrary to the mentioned studies (more references could be added). They suggest that reduced raindrop freezing explains this, but previously mentioned that latent heating was the same. How can this be since latent heat is released from droplet condensation? Were the drop sizes smaller? Was there more snow?

Response:

Thanks for these questions. We will deal with them one by one.

(A) Regarding the latent heat.

For clarity, we have used the temporal variation of the vertical profiles of peak latent heating (Figure 12, revised version) to make comparison of latent heat between both simulations during the whole duration of the thunderstorm. The latent heat shown in Figure 12 results from both condensation and freezing. Related analysis have been modified in several parts, for example:

Lines 324-329: "**Under polluted condition, more aerosols could be activated into cloud droplets and more water vapor condenses onto these droplets, leading to large cloud water content and small droplet size (Lynn et al., 2007; Wang et al., 2011; Zhao et al., 2015; Jiang et al., 2017). Thereby, relatively more latent heat of condensation released in the P-case where large cloud water content exists, which can be seen in the vertical distribution of peak latent heat (Figure 12).**"

Lines 331-334: "**Under polluted condition, cloud droplets with smaller mean-mass radius are too small to be converted into raindrops. As a consequence, the rainwater mass mixing ratio is less in the polluted case compared to the continental one (Figure 10d).**"

Lines 371-373: "**In this study, the graupel content was higher in the C-case, probably owing to higher rainwater content and corresponding raindrop freezing.**"

(B) Regarding the drop size and snow contents.

We have added domain-averaged properties of different hydrometeors in Table 3 (revised version). The information of snow is shown in Table R1 and Figure R2. The size of raindrops in the P-case is larger, which is also be found in Wang et al. (2011), probably resulting from the melting of ice-phase particles. By collecting droplets and ice-phase particles, the aggregation of snow in the simulation is partially similar to the

accretion of graupel (Zrnic et al., 1993; Ziegler et al., 1985). The snow content is also less in the P-case (Figure R2a, R2b), while there is no significant difference of domain-averaged mean-mass radius of snow between the P- (421.1 μm) and C-case (375.9 μm, Table R1). The single graupel category, which has variable density in the microphysical scheme, represents a spectrum of particles ranging from high-density frozen drops (or small hail) to low-density graupel (Mansell et al., 2010), therefore, could better represent mixed-phase processes. Since there is little difference of number concentration and mean-mass radius compared to the graupel and ice crystal, we would add these to the supplement if necessary.

Table R1. Domain-averaged Properties of Hydrometeors.

	Number Concentration (10^3 kg^{-1})		Mean-mass Radius (μm)	
	C-case	**P-case**	**C-case**	**P-case**
Cloud droplets	3930	7910	6.5	6.1
Rain drops	0.069	0.031	154.1	179.9
Ice Crystals	2280	3850	3235.8	2994.9
Graupel	0.028	0.012	322.4	479.5
Snow	4630	3880	375.9	421.2

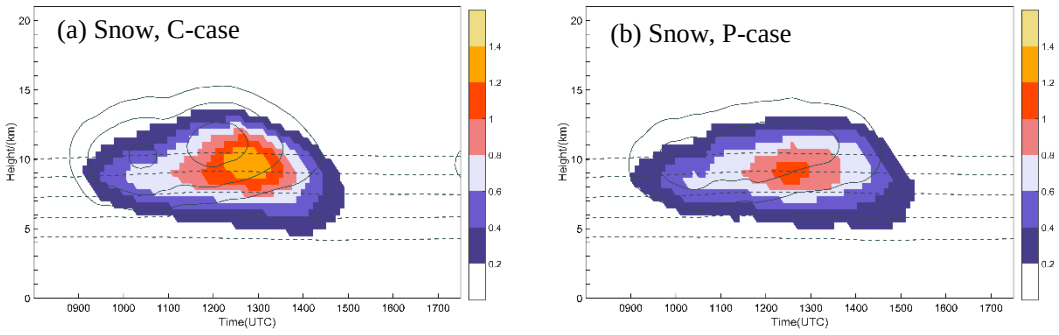

Figure R2 (a)-(b) Temporal variation of the vertical profiles of domain-averaged mass mixing ratio (g kg^{-1}, shaded) and number concentration (kg^{-1}, solid lines) of (a) snow in the C-case, (b) snow in the P-case. Contour levels in (a)-(b) for snow are 1.5×10^4, 3.0×10^4, 5.0×10^4 kg^{-1}. The 0 °C, -10 °C, -20 °C, -30 °C and -40 °C isotherms are shown by the dashed gray lines in (a)-(b).

280: The authors then note that the maximum amount of graupel in the mature stage is higher in P versus C, but don't explain why the results have changed.

280+ It is incorrect to claim that there are any appreciable differences in the dissipating stage, based on the numbers given.

Response:

Sorry for the ambiguity. The area we chose in the initial manuscript was too small, so the different stages could not be well matched in different cases. We have re-analyzed the microphysical processes after chosen a larger region (denoted in Figure 4d, revised version), so that the microphysical processes can be analyzed entirely. In the larger analyzed region, domain-averaged properties and related analysis of graupel have been added in Table 3 and Part "**4.2 Microphysical properties of multicell"** (revised version, lines 362-382).

295: The short paragraph is a conclusion, rather than a result.

Response:

Thanks for the reminder. We have rephrased this paragraph. (Revised version, lines 383-386)

305: How is dipolar charge structure more consistent with previous observations. Please tell the reader the difference between dipolar and simple dipoles/tripoles.

Response:

Thanks for this suggestion. We have added related references and the description of charge structure. (Revised version, lines 409-418)

310: negative charge region in which simulation?

Response:

Thanks for this reminder. We have clarified this sentence as follows: "**The negative charge region in the upper level (12-15 km) for the P-case resulted from collisions of graupel particles with smaller ice crystals and snow particles (Fig. 14d)**". (Revised version, lines 422-424)

320: Why do graupel and hail partices charge negatively?

Response:

Thanks for this comment. We have added related reference to explain as follows: "**According to Saunders and Peck (1998) non-inductive charging curve, graupel charges negatively within regions of relatively weak updrafts (< 5 m s^{-1}) and lower liquid water content (LWC), forming a negative charge region at 4-8 km in the P-case.**" (Revised version, lines 436-439)

340: Very hard to understand the sentence structure.

Response:

Sorry for the ambiguity. This sentence has been modified in the revised version, lines 452-454.

350: More recent references needed.

Response:

Thanks for this suggestion. We have added recent references as follows: "**Previous studies showed that larger vertical velocities were driven by increased microphysical latent heating. (Wang et al., 2011; Mansell and Ziegler, 2013;**

Altaratz et al., 2017; Fan et al., 2018; Li et al., 2019)." (Revised version, lines 335-337)

355:

"Considering that both cases have rather high CCN concentration, there would not be much difference between them in condensation." So, then what makes them difference. (By the way, I am not sure I believe this; more information is needed comparing mass, not just concentrations -- but we're still left with the question of why?).

Response:

Thanks for this question. For clarity, we have used the temporal variation of the vertical profiles of peak latent heating (Figure 12, revised version) to make comparison of latent heat between both simulations during the whole duration of the thunderstorm. The latent heat shown in Figure 12 results from both condensation and freezing. For the condensation latent heat, we modified the related analysis in Part "**4.2 Microphysical properties of multicell",** for example:

Lines 323-329: "**Under polluted condition, more aerosols could be activated into cloud droplets and more water vapor condenses onto these droplets, leading to large cloud water content and small droplet size (Lynn et al., 2007; Wang et al., 2011; Zhao et al., 2015; Jiang et al., 2017). Thereby, relatively more latent heat of condensation released in the P-case where large cloud water content exists, which can be seen in the vertical distribution of peak latent heat (Figure 12).**"

For the frozen latent heat, the related analysis has been added as follows: "**the maximum of peak latent heat in the P-case occurs above 10 km at 09:30 UTC (Figure 12), indicating that more cloud droplets are lifted to the upper levels (< -40 °C) and converted into ice crystals at the beginning stage of the thunderstorm. … The high value of latent heat existed in the higher levels (above 10 km) reveals a large amount release of frozen latent heat. Previous studies also**

found that elevated aerosol loading contributed to the increasing frozen latent heat (e.g., Khain et al., 2005; Lynn et al. 2007; Storer et al., 2010; Li et al., 2017)."(Revised version, lines 349-357)

365: Section 4.5: Why is it a separate section and not integrated within the text?

370: "In the meanwhile" refers to when?

390: What simulation becomes much larger at 9:30 UTC?

Response:

Thanks for the comment. As mentioned before, we re-analyzed the microphysics along with further electrification and lightning activities of this thunderstorm, in the region denoted in Figure 4d. The re-analyzed results still suggest that under polluted condition lightning activity is significantly enhanced, while the delay of the first discharging in the C-case is not obvious. And we would delete this part in the revised version.

405: Please discuss what are the microphysical processes effected.

Response:

Thanks for the comment. The discussion of microphysical processes have been added. (Revised version, lines 471-480)

415: Is that heat of fusion rather than latent heat?

Response:

Thanks for this question. The latent heat shown in Figure 12 (revised version) results from both condensation and freezing.

425: The paragraph beginning with "Compared to C-case" has a contradiction.

Shouldn't ice and graupel grow more quickly due to coalescence? You just pointed out that "it was not noted."

Response:

Thanks for this comment. As mentioned before, we re-analyzed the microphysics along with further electrification and lightning activities of this thunderstorm, in the region denoted in Figure 4d. The re-analyzed results still suggest that under polluted condition lightning activity is significantly enhanced, while the delay of the first discharging in the C-case is not obvious. And we would delete related description in the revised version.

675: Figure 5: How are these vertical profiles calculated -- over what volume?

Response:

Thanks for this question. We have clarified as follows: "**Figure 10a-10h show the temporal variations of the vertical profiles for different hydrometeors. For each quantity, the mass mixing ratio and number concentration of hydrometeors are averaged horizontally over the analyzed region at a given altitude.**" (Revised version, lines 312-315).

685: Please better define "domain" in the figure caption of Figure 6.

Response:

Thanks for reminder. We have defined "domain" as "**the impacts of aerosol on lightning activity will only be evaluated in the southeastern Beijing area (39.4 °N-40.6 °N, 116.0 °E-117.5 °E, shown in Fig. 4d; here on, 'domain' for short)**" (revised version, lines 252-254) and denoted in the Figure 4d (revised version).

695/705: Figure 7 and 8: the word "main" is not clearly defined. Might differences also

be shown?

Response:

Thanks for reminder. We have clarified in Figure 14 and 15 as: "**simulated variables**" (revised version).

1260

710: What is "the location shown in Fig. 2?"

Response:

Thanks for reminder. We have clarified in Figure 16 (revised version).

References

Fan J, Rosenfeld D, Zhang Y, et al. Substantial convection and precipitation enhancements by ultrafine aerosol particles[J]. Science, 2018, 359(6374): 411-418.

Gustafsson, N., Janjić, T., Schraff, C., Leuenberger, D., Weissmann, M., Reich, H., et al. (2018). Survey of data assimilation methods for convective scale numerical weather prediction at operational centres. Quarterly Journal of the Royal Meteorological Society, 144, 1218–1256. https://doi.org/10.1002/qj.3179

Li Z, Wang Y, Guo J, et al. East asian study of tropospheric aerosols and their impact on regional clouds, precipitation, and climate (EAST-AIRCPC)[J]. Journal of Geophysical Research: Atmospheres, 2019, 124(23): 13026-13054.

Sun, J., Xue, M., Wilson, J. W., Zawadzki, I., Ballard, S. P., Onvlee Hooimeyer, J., et al. (2014). Use of NWP for nowcasting convective precipitation: Recent progress and challenges. Bulletin American Meteorological Society, 95, 409–426. https://doi.org/10.1175/BAMS-D-11-00263.1

Zrnic D S, Balakrishnan N, Ziegler C L, et al. Polarimetric signatures in the stratiform region of a mesoscale convective system[J]. Journal of Applied Meteorology and Climatology, 1993, 32(4): 678-693.

Interactive comment on "Aerosol Effects on Electrification and Lightning Discharges in a Multicell Thunderstorm Simulated by the WRF-ELEC Model" by Mengyu Sun et al.

M. Sun et al.

sunmengyu16@mails.ucas.edu.cn

Reply to Referee 2

General Comments:

The submitted paper is directed to study the effects of CCN concentration on lightning activity. Although the hypothesis of a link between the lightning frequency and CCN concentration is not new there are still only limited numbers of papers investigating the physical processes responsible for these links. However, the results of these studies are not unambiguous. Therefore, any further analysis in this direction (as is in the submitted paper) is well come for the scientific community. To reveal the effect of the CCN on microphysics and cloud dynamics and their impact on thunderstorm electrification and lightning, the authors present the results from numerical simulations with two different CCN concentrations: a polluted case (P-case) and a continental case (C-case). The Weather Research and Forecasting (WRF) Model coupled with bulk lightning model and a two-moment bulk microphysics scheme used to simulate a multicell thunderstorm is adequate for the aim of their study. The title corresponds to the content of the paper. The abstract is informative. Many recent and appropriate papers are cited in the Introduction. The paper as a whole is well structure. Most of the figures are of good quality. The analysis of the results of model simulations is directed to reveal the physical processes responsible for the significantly higher frequency of lightning in the P-case, as well as the earlier start of the discharge in the C-case. However, some conclusions are based on assumptions, rather than on detailed analyses of the corresponding numerical simulation results. A more comprehensive discussion, related to the mechanism by which the differences (due to the impact of CCN) in microphysics,

thermodynamics, and cloud dynamics affect the electrification of clouds, is required. Additional information, figures and analyses are needed to convince the reader of the validity of the drawn conclusions. Based on the above I recommend the submitted paper to be revised taking into account the specific comments and recommendation below.

Response:

We greatly appreciate the instructive and constructive comments. We have studied them carefully and have addressed them in the revised manuscript. Below are the point-by-point responses to the reviewer's comments.

Specific Comments:

3. Model overview

It is necessary to provide additional information related to the numerical model and design of simulation, and not just direct the reader to the relevant papers.

On Ln 141-143 it is written: "The initiation of cloud droplets (both for cloud base and in-cloud) uses an expression based on Twomey (1959)." Please explain a little bit more and give the empirical expression proposed by Twomey (1959). Since the CCN spectra is approximated by power dependence on supersaturation using two time- and location-dependent coefficients, what were their specific values that you used in numerical simulations of C- and P-case? Does supersaturation threshold specified above which CCN number do not increase in the model?

Response:

Thanks for this comment. This comment contains 3 questions. We'll deal with them one by one.

(A) Regarding the description related to the initiation of cloud droplets:

The initiation of cloud droplets is based on Twomey (1959) and adjusted by Mansell et al. (2010). The number concentration initiated at cloud base is: $C_{N,cb} =$

$\frac{1}{\Delta t}10^6(10^6C)^{2/(k+2)}[\frac{1.63w^{3/2}}{kB(3/2,k/2)}]^{k/(k+2)}$, where C is the assumed CCN concentration, w is the updraft speed, B is the beta function, and k is the exponent in the relation $N_{CCN} = CS_w^k$, S_w is the supersaturation with respect to liquid water. Within the cloud, the initiation rate C_N is: $C_N = CkS_w^{k-1}\mathbf{V} \cdot \nabla S_w$.

(B) Regarding the CCN spectra:

We have added related information in the revise manuscript, for example:

Lines 150-153: "**The CCN concentration is predicted as a bulk activation spectrum and initially mixed well vertically, following Mansell et al. (2010): $N_{CCN} = CCN \times S_w^k$, where CCN is the assumed CCN concentration, S_w is the supersaturation with respect to water, and k = 0.6**". And the assumed CCN concentration for both cases have been clarified in the revised version (lines 225-233).

(C) Regarding the supersaturation S_w:

For the first appearance of S_w at grid point, the mass of initiated droplets is calculated either by an iterative saturation adjustment or by one-step adjustment in Klemp and Wilhelmson (1978). Within the cloud, the vertical gradient of supersaturation is replaced with full gradient [$w(\partial S/\partial z) \rightarrow \mathbf{V} \cdot \nabla S_w$]. In this study, we apply no supersaturation adjustment and the threshold of that do not increase with CCN number in the model.

Ln 145-147 it is written:

"Non-inductive charge separation resulting from rebounding collisions between graupel-hail and snow-cloud ice are all parameterized (Mansell et al., 2005)". Instead of just directing the reader to the relevant paper, it is necessary to give additional brief information about the calculation of magnitude and sign of separated charge at non-inductive interaction of the hydrometeors. It is useful to be noted that the sign of the separated charge based on the results in Saunders and Peck (1998) depends not only on the cloud water content but on in-cloud temperature and on rime accretion rate, which in turn additionally depends on the mean fall velocity of riming ice particles. And it is also not correct that in Mansell et al., 2005 rebounding collisions between graupel-hail

and snow-cloud ice are taken into account. In Mansell et al, 2005 it is written Charge separation rates are calculated for rebounding collisions of graupel with cloud ice and aggregate" and "No charge separation is calculated for rebounding collisions between snow aggregates and ice crystals". You should mention the rebounding collisions between various ice-phase particles (ice, graupel, snow, hail), which resulting in the separation of charge in the frame of your numerical simulations.

Response:

We agree to the suggestion and we have optimized the description according to the suggestions.

(A) Regarding additional information about the calculation of non-inductive charge separation:

We have added in the revised manuscript. (Revised version, lines 156-161)

(B) Regarding the rebounding collisions in Mansell et al. (2005):

Sorry for the inaccuracy. This description has been revised as suggested. (Revised version, lines 166-170)

Give also additional information related to the discharge model parametrization – i.e. how the electric field is simulated, what is the prescribed breakdown threshold, the values of the cylinder cross section C in eq.1, how the net total charge density is altered after the discharge and others. In section 4.5, where you analyze the reasons leading to delay in charge onset in P-case you pay special attention to the area in which the total charge density is > +0.1 nC m^{-3} or < -0.1 nC m^{-3}. It can be assumed that this is related to some basic assumption at lightning parametrization in the numerical model. If so, it must be also explained in section 3. Model overview.

Response:

Thanks for this comment. We have added the description as suggested. For example:

Lines 184-186: "**A flash would be initiated when the electric field exceeds a breakdown threshold, which variants of vertical electric profile of Dwyer (2003) at a model grid point**".

Lines 198-199: "**C the cylinder cross sectional area (set in the following simulations to radius R = 12 km (Fierro et al., 2013))**".

Lines 188-190: "**If the space charge magnitude at a grid point exceeds a specific space charge threshold (0.1 nC m^{-3} herein), this grid point will be involved in discharge within the cylinder during this time step.**"

Please, explain also how the effective radius of various hydrometeors (presented in Fig.7) is calculated.

Response:

Thanks for this suggestion. The related method has been added as follows: "**The domain-average mean-mass $radius_h$ of hydrometeors in Table is calculated following Eq. (7):**

$$radius_h = \left[\frac{1}{c_h} \times \frac{Sum(\rho_{air}(i,j,k) \times q_h(i,j,k))}{Sum(\rho_{air}(i,j,k) \times n_h(i,j,k))}\right]^{1/3}, \quad (7)$$

where ρ_{air} is the air density, and c_h, q_h, n_h are the density, mass concentration, and number concentration of hydrometeor species *h* (Mansell et al., 2010), respectively." (revised version, lines 315-319) We noted that this is domain-averaged mean-mass radius instead of "effective" radius. So we modified it to "domain-averaged mean-mass radius".

The information on the initial and boundary conditions given on line 166-168, namely: "The nested model configuration for the simulations are shown in Table 1. The 1 °×1 °NCEP GFS (Global Forecast System) data is used to establish the initial and boundary conditions." is insufficient. You should specify the starting time and the hourly interval (1h, 3h, or more hours) updates of GFS data used for your numerical

simulations. I do not understand why do you use 1 °×1 ° NCEP GFS data instead of 0.25 °×0.25 ° (or at least 0.5 °×0.5 °) GFS data. And please explain, how do you perform nesting technique from a domain with a resolution of roughly 100 ×100 km to a domain with a resolution of 6 ×6 km?

Response:

Thanks for the comment. This comment contains 3 suggestions. We'll deal with them one by one.

(A) Regarding the information on the initial and boundary conditions:

We checked the simulations and found that 0.5 °×0.5 ° NCEP GFS data was used for the initial and boundary conditions. We have corrected this mistake in the revised version.

(B) Regarding the starting time and the hourly interval updates of GFS data:

In our revised version, we have added the related information. (Revised version, lines 216-220)

(C) Regarding how to perform nesting technique:

The WRF Preprocessing System (WPS, shown in Figure R1) is used to configure real-data simulations. First, we use "geogrid" program to define dimensions and horizontal resolution of domains (here we set the 6 km and 2 km nests). "Geogrid" also provides values for static fields at each model grid point. And then, the "ungrib" program is deployed to read GRIB files (a WMO standard file format for storing regularly-distributed fileds) and extract meteorological fields (Vtables are used to extract fields). Finally, we use the "metgrid" program to interpolate meteorological data (extracted by ungrib) to simulation domains (defined by geogrid) horizontally. More details could be found at: https://www2.mmm.ucar.edu/wrf/users/

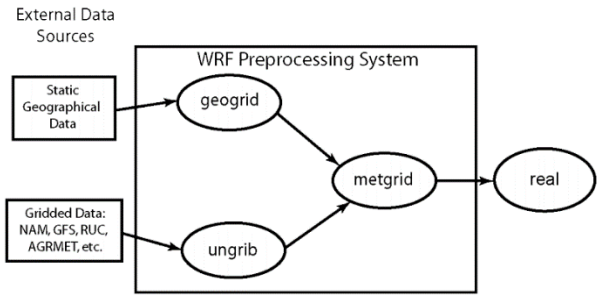

Figure R1 WPS program flowchart

4. Results

Before presenting the detailed analysis of the specific results, it would be useful to give the most general information about the simulated thunderstorms with two different CCN concentrations - at least the moment of the beginning of the formation of both simulated thunderstorms, their life time, the cloud base height, the maximum of cloud top height, the maximum updraft velocity, the amount of precipitation and others.

Response:

Thanks for this suggestion. We have added details of the simulated thunderstorms (Revised version, Table 2, 4). The precipitation information has been added as well. (Revised version, lines 254-272; Figure 6, 7)

4.1 Radar reflectivity and lightning flashes of multicell

The presented results in Fig. 2 and Fig 3 reveal that the numerical model used for the study of CCN impact on lightning activity adequately simulates some of the main manifestations of the real observed multicell thunderstorm. However, on the basis of this information alone, it is not possible to draw any other conclusions, including the statement in the last section, namely:

Ln 405-406 “The simulated distributions and spatio-temporal development of radar reflectivity are in overall agreement with observations.” For this purpose, it is necessary to present at least observed radar reflectivity as a function of height in different stages of thunderstorm development with a 1.5-hour delay. And I assume that conclusion would be that the observed radar reflectivity is in agreement with simulated radar

reflectivity only in the polluted case.

Response:

Thanks for this suggestion. We have presented the comparison of radar reflectivity for the observation and simulations at analyzed time (Figure 5 in revised version,), and added related description as follows: "**According to the morphology and intensity of the radar echo, the observed radar reflectivity is in better agreement with simulated radar reflectivity only in the polluted case.**" (Revised version, lines 247-249)

Since "the impacts of aerosol on lightning activity will only be evaluated in the southeastern Beijing area (116.0 ℉-117.5°E)" (Ln 193-194) for clarity, denote in Fig. 2 the regions for which the results are analyzed. Please, explain how the presented in-cloud characteristics were averaged horizontally and in which region the lightning frequencies, shown in Fig.3 have been detected or simulated. It is useful also to specify the average rainfall only in the analyzed region?

Response:

Thanks for this comment. This comment contains 3 suggestions. We'll deal with them one by one.

(A) Regarding the analyzed region:

We have denoted in Figure 4d (revised version) the regions where the results are analyzed. And the spatial distributions of BLNET stations have been added in Figure 1 (revised version).

(B) Regarding the comparison of rainfall in the analyzed region:

The comparison of rainfall has been added in the revised version. (Lines 254-272; Figure 6, 7)

(C) Regarding the details of horizontal average process:

We have added in the revised manuscript as follows: "**For each quantity, the mass mixing ratio and number concentration of hydrometeors are averaged horizontally over the analyzed region at a given altitude.**" (Revised version, lines 312-314)

Ln 199-202

"According to the evolution of radar reflectivity and lightning activity, the thunderstorm was divided into four periods: the beginning stage (before 11:00 UTC), the developing stage (11:00-12:30 UTC), the mature stage (12:30-13:30 UTC) and the dissipating stage (after 13:30 UTC) of the thunderstorm" It is necessary to explain what the criteria were for determining the time intervals of the four stages of real and simulated development of a thunderstorm. I do not agree that lightning activity is suitable to be used for this purpose. An idea about the stages of thunderstorm development can be obtained for example on the basis of the evolution of heights of radar reflectivity 5 dBz and 45 dBz, the maximum radar reflectivity with the moment and height of its achievement. That is why I recommend to add such information (or something else) especially for the simulated C- and P-case. Based on chosen criteria, please give information for the corresponding four periods in the simulated C- and P-case and denote on the time scales in Fig.3b, Fig.5 (a-j), Fig.6 (a-d) the intervals of the mature stage in both simulated cases. This will facilitate to follow the analysis of the presented results and the conclusions drawn.

Response:

Thanks for this suggestion. In this study, the life cycle of the thunderstorm is determined according to the radar echo and lightning activities (Van Den Broeke et al., 2008; Kumjian et al., 2010, Liu et al., 2021). For the developing stage, the storm is accompanied with strengthened intensity and enlarged scale, with the lightning frequency increasing gradually. With regard to the mature stage, the maximum radar reflectivity at least reach 45 dBZ and the strong convective cell is formed, and the 15 dBZ echo top evaluate and the lightning frequency increase dramatically. As for the

dissipating stage, the intensity of the storm is weakened with the 15 dBZ decreased, and the lightning frequency decreased remarkably. We have added the criteria and the real and simulated developments of the thunderstorm has been added. (Revised version, lines 277-279, Table2)

The conclusions made on the basis of the analysis of the results presented in Fig. 4, namely

Ln 217-221"There is no lightning initiation for the P-case at the beginning of the thunderstorm (08:30-09:30 UTC, Fig. 4a), however, all categories of lightning are initiated in the C-case, indicating that the first discharging is delayed under polluted condition." are not unambiguous. It is necessary to indicate whether the delay of lightning initiation in the simulated P-case is due to the delay in the development of the thunderstorm or if the delay is due to another cause. For that reason, it would be useful if you present at least the evolution of cloud top height in P- and C-case starting from the early moment of thunderstorm formation before lightning initialization.

Response:

We appreciate this suggestion. In light of the following comment on the gap in the maximum radar reflectivity, we have analyzed the radar reflectivity and precipitation (Figure 6, 7, revised version) at the beginning stage of the thunderstorm for the observation and both simulations. Since the observed radar reflectivity during 11:00-11:24 UTC is missing, so Figure R2 shows the radar echo before and after 11:15 UTC (09:45 UTC in simulations) for comparison. In the early stage of the thunderstorm, the radar echo for the P-case is relatively similar with these of the C-case. We realized that the area we chose in the initial stage was too small. The extra cell in figure 5j (initial version) probably because that the previous selected area did not include the cell in the C-case. Therefore, we have enlarged the region (shown in Figure 4d, revised version). The microphysics along with further electrification and lightning activities of this thunderstorm have been re-analyzed. With such improvements, we believe the analysis of the physical processes is much appropriate for explaining the difference in the

electrification and discharging in both simulated cases. The dynamic-thermodynamic processes do affect the development of thunderstorm significantly (e.g. Williams et al., 2005; Guo et al., 2016; Wang et al., 2018; Zhao et al., 2020), the re-analyzed results still suggest that under polluted condition lightning activity is significantly enhanced. While the delay of the first discharging in the C-case is not obvious. So we will delete this Part "4.5 Delay of first flash in polluted case" in the revised version. The detailed analysis of microphysical processes will be given in the following reply.

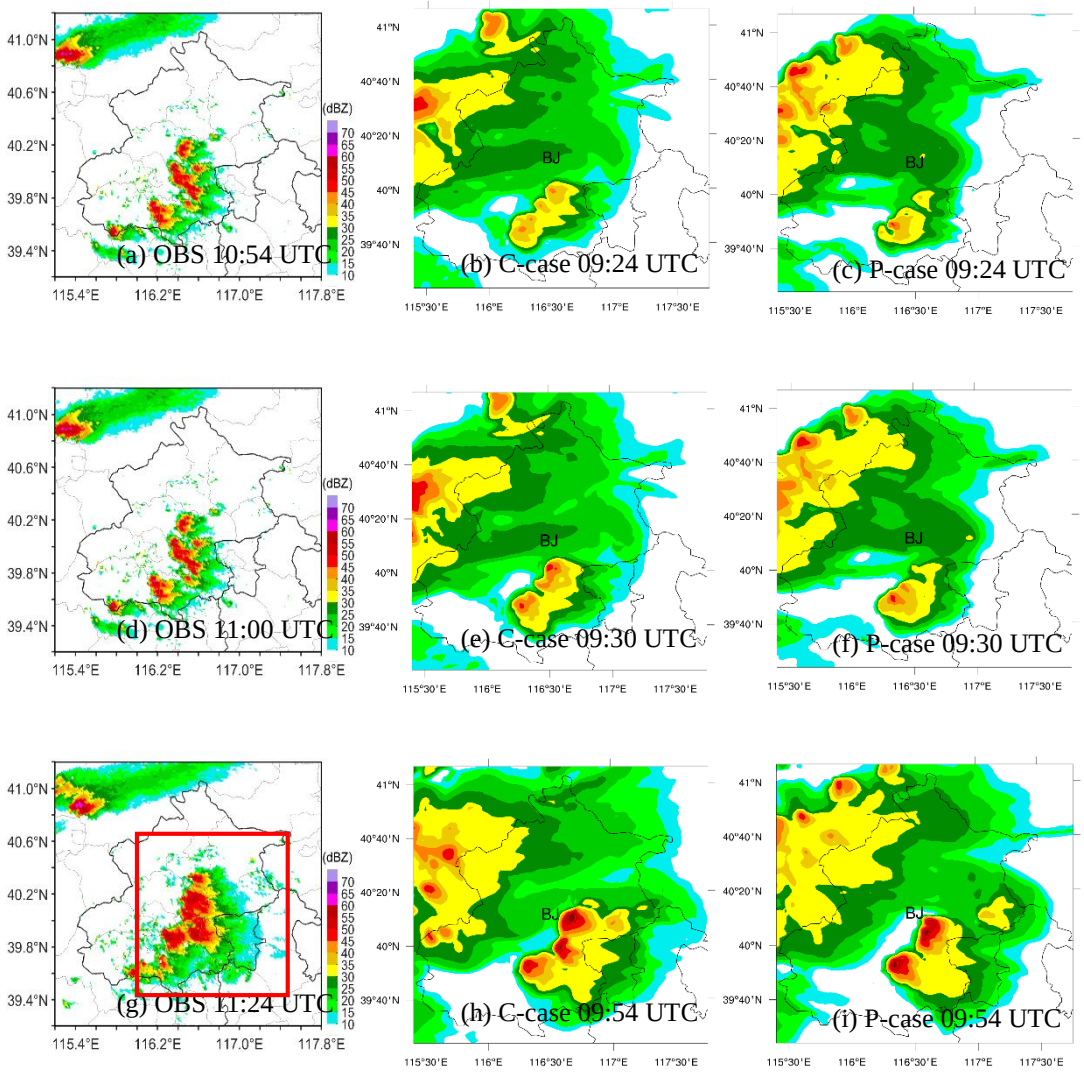

Figure R2 Radar reflectivity (unit: dBZ) between observation and simulation for the C- and P-cases, the simulation was earlier than observation about 1.5 h. (a), (d), (g) Observation at 10:54 UTC, 11:00 UTC and 11:24 UTC. (b), (e), (h) Simulation for the C-case at 09:24 UTC, 09:30 UTC and 09:54 UTC. (c), (f), (i) Simulation for the P-case at 09:24 UTC, 09:30 UTC and 09:54 UTC, respectively. The red rectangle in Fig. R2g denotes the region where the simulated results are

analyzed in this study.

4.2 Microphysical properties of multicell

In Fig. 5 the vertical profiles of averaged horizontally mass mixing ratios and number concentration for different categories of hydrometeors as a function of time are shown for C- and P-case. No sound conclusions can be drawn for the impact of CCN concentration on cloud dynamics and microphysics on the basis of the horizontally averaged values alone. Information related to the corresponding maximum values, the height and time of their achievements has to be presented. For detailed analysis, it is also necessary to show additionally plots with the maximum values of updrafts and downdrafts as a function of time and height. I assume that the isolines of updrafts and downdrafts presented in Fig. 5i and 5j are horizontally averaged values, because they are too low for thunderstorms with an overshooting top, producing lightning. Please discuss also the reason for a gap in maximum radar reflectivity between 9:20 UTC and 10:00 UTC and between 10:30 UTC and 11:15 UTC in Fig. 5i. It will be also helpful if somehow the interval of the mature stage on the time scales in any of the plots in Fig. 5 is indicated. Why are there no plots of the mass mixing ratios and number concentration of snow and hail, especially considering that in section 4.3 the charge carried by these ice- particles is presented and discussed? And what about the simulated precipitation in C- and P-case? Please, add appropriate information and plots for example, peak rainfall rate (mm/h) as a function of time, total rainfall volume and others. Without such information, the analysis of the physical processes responsible for the difference in lightning frequency in both simulated thunderstorm cases is limited and the conclusions are not reliable.

Response:

Thanks for the comment. This comment contains 4 questions. We'll deal with them one by one.

(A) Regarding the information related to the maximum values, the height and time of updrafts and downdrafts

We have added the related figures and analysis. (Revised version, Lines 336-343; Figure 10i-10j; Table 4)

(B) Regarding the gap in maximum radar reflectivity between 9:20 UTC and 10:00 UTC and between 10:30 UTC and 11:15 UTC in Fig. 5i (initial version)

As mentioned before, we have re-analyzed the microphysical processes of the thunderstorm in the region denoted in Figure 4d. (Revised version, Part "**4.2 Microphysical properties of mulicell**", lines 309-385)

(C) Regarding to the mass mixing ratios and number concentration of snow and hail

The information of snow and hail have been displayed in Figure R3, R4 and summarized in Table R1. Yes, snow and hail are involved in the electrification. By collecting droplets and ice-phase particles, the aggregation of snow is partially similar to the accretion of graupel (Zrnic et al., 1993; Ziegler et al., 1985). The snow content is also less in the P-case (Figure R3a, R3b), while there is no significant difference of domain-averaged mean-mass radius of snow between the P- (421.1 μm) and C-case (375.9 μm, Table R1). The single graupel category, which has variable density in the microphysical scheme, represents a spectrum of particles ranging from high-density frozen drops (or small hail) to low-density graupel (Mansell et al., 2010), therefore, could better represent mixed-phase processes. After 12:00 UTC, the mean-mass radius of snow in both cases tend to increase (Figure R4a), which probably comes from the ice-phase particle conversion. Figure R3c-R3d display the temporal variations of the vertical profiles for hail in both cases. It can be seen that the difference of mixing ratio of hail between the two cases is not as obvious as that of graupel and ice crystals, during 10:00-13:00 UTC. The mean-mass radius of hail is slightly larger in the P-case (Table R1, Figure R4b). Small hail could be represented by frozen drops in the graupel category, whereas the hail category tends to represent larger hail (Bruning et al., 2007), this probably explains the little difference of hail between the two cases. Since there is little difference of number concentration and mean-mass radius compared to the graupel and ice crystal, we would add these to the supplement if necessary.

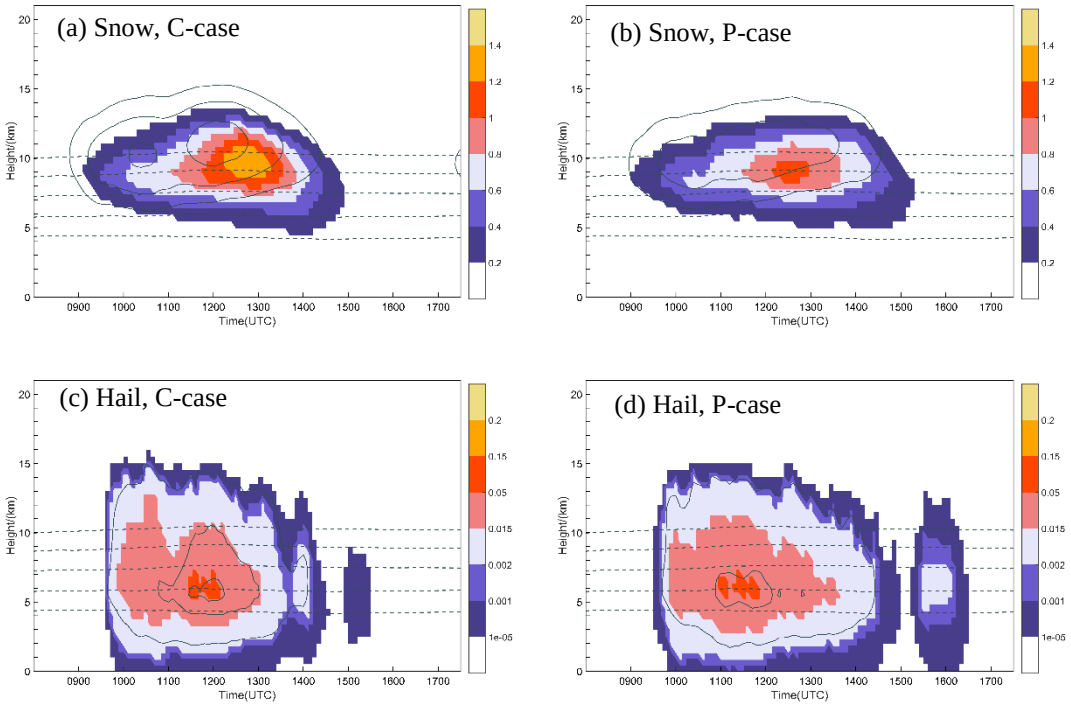

Figure R3 (a)-(d) Temporal variation of the vertical profiles of domain-averaged mass mixing ratio (g kg^{-1}, shaded) and number concentration (kg^{-1}, solid lines) of (a) snow in the C-case, (b) snow in P-case, (c) hail in the C-case, and (d) hail in the P-case. Contour levels in (a)-(b) for snow are 1.5×10^4, 3.0×10^4, 5.0×10^4 kg^{-1}, and for hail are 0.1, 1.0, 2.0 kg^{-1}. The 0 ℃, -10 ℃, -20 ℃, -30 ℃ and -40 ℃ isotherms are shown by the dashed gray lines in (a)-(d).

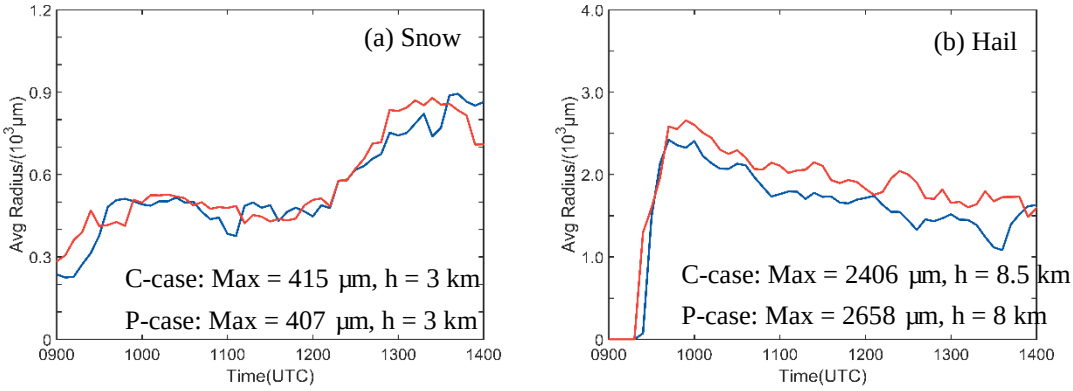

Figure R4 Temporal variation of domain-averaged mean-mass radius for the different hydrometeors. (a) snow, (b) hail. The red lines represent the P-case and the blue lines represent the C-case.

Table R1. Domain-averaged Properties of Hydrometeors.

	Number Concentration (10^3 kg^{-1})		Mean-mass Radius (μm)	
	C-case	**P-case**	**C-case**	**P-case**
Snow	4630	3880	375.9	421.2
Hail	0.00005	0.00004	1019.1	1248.6

(D) Regarding to the comparison of precipitation in the simulated C- and P-cases.

According to this suggestion, we have provided the comparison of precipitation for the observation and both simulations. (Revised version, lines 254-272; Figure 6, 7).

I do not understand for what reason the authors have decided first to consider the profile of total charge density and the charge carried by different ice-particles during the mature stage, then in the initial stage and without any attention to the impact of microphysics and dynamics of simulated clouds on their electrification during the maximum of lightning frequency. I do not think that it is appropriate to have separate sections - 4.4 Convective strength and 4.5 Delay of first flash in polluted case. All this can be presented in one section 4.3. The relationship between electrification, microphysics and dynamics. Again, the analysis presented in this section is cursory, often based on assumptions rather than on a profound investigation of the relation between microphysics, dynamics and thunderstorm charging. In order to get an idea about the formation of the charge structure during the different stages of thunderstorm development, it is appropriate to present horizontally averaged total charge density as a function of height and time, indicating for each of the stages of cloud development the maximum (minimum) positive (negative) total charge density together with the height and the moment of their achievement. Consideration of these results together with the results shown in Fig. 5 can give a general idea of the relationship between the mass of the ice-particles, updraft and downdraft velocity and time-height distribution of charge density in the polluted and in the continental case. In this analysis, it may be

useful to pay attention to the time and amount of precipitation. And then to analyze the impact of microphysics and dynamics on thunderstorm electrification in 3 specific moments sequentially: at the initial moment of thunderstorm development (Fig. 11 and Fig.12), during the period of maximum lightning frequencies (it is necessary to show additionally appropriate figures) and finally during the mature stage (Fig. 7 and Fig.8) in the two simulated C- and P-cases. In my opinion, such a sequence of considerations would allow more detailed analysis to be made to clarify the processes responsible for the significantly higher lightning frequency in the P-case and the earlier onset of the discharge in the C-case. However, more comprehensive analyses have to be done, rather than only listing the results in the presented figures. For this purpose, it would be useful to look (at some specific moments of thunderstorms development) the profiles of the maximum updraft velocity and the mass of some hydrometeors related to thunderstorm charging.

Response:

We appreciated these valuable suggestions. This comment contains 2 suggestions. We will deal with them one by one.

(A) Regarding the analysis of charge density as a function of height and time.

We have added the temporal variation of the vertical profiles of peak positive (negative) charge density in the revised version (Figure 13). The WRF-ELEC outputs the total charge density after each discharge, so we chose to use peak charge density instead. In addition, we have added the related description. (Revised version, lines 388-398)

(B) Three specific moments: the initial moment, the mature stage, and the period of maximum lightning frequencies.

As mentioned before, we have re-analyzed the microphysics along with further electrification and lightning activities of this thunderstorm, in the region denoted in Figure 4d. The re-analyzed results still suggest that under polluted condition lightning activity is significantly enhanced, while the delay of the first discharging in the C-case

is not obvious. And we would delete the Part "4.5 Delay of first flash in polluted case" in the revised version.

As shown in Figure 13 (revised version), the domain-averaged peak positive (negative) charge structures at the mature stage are similar with the period of maximum lightning frequency for both cases. And we have analyzed the vertical cross sections of simulated variables during the period of maximum lightning frequency (shown in Figure R5, R6, and R7), and found that the relationship between hydrometeors and electrification may not differ very much from the mature stage. For the total net space charge density, the maximum of positive charge density in the P-case (more than +1 nC m^{-3}, Figure R5a) is much higher than that in the C-case (less than +0.5 nC m^{-3}, Figure R6a), during the period of maximum lightning frequency. The collisions between ice particles and snow particles could partially explain the strong positive charge center located at 10-14 km in the P-case (Figure R5b). Less ice-phase particles appear in upper level in the continental case, corresponding to a relatively weaker charge center. In the polluted case, graupel and hail were charged negatively (Figure R7b, Saunders and Peck, 1998) with lower LWC, forming a negative charge center at 9km (< -20 ℃, shown in Fig. R5a). The appearance of more ice-phase particles in upper level, increasing ice crystals number and mean-mass radius of graupel, together led to greater charge densities and as a consequence to stronger electric field intensities. So we have only kept the related analysis at the mature stage in the revised version. (Lines 387-459, Figure 14, 15, and 16)

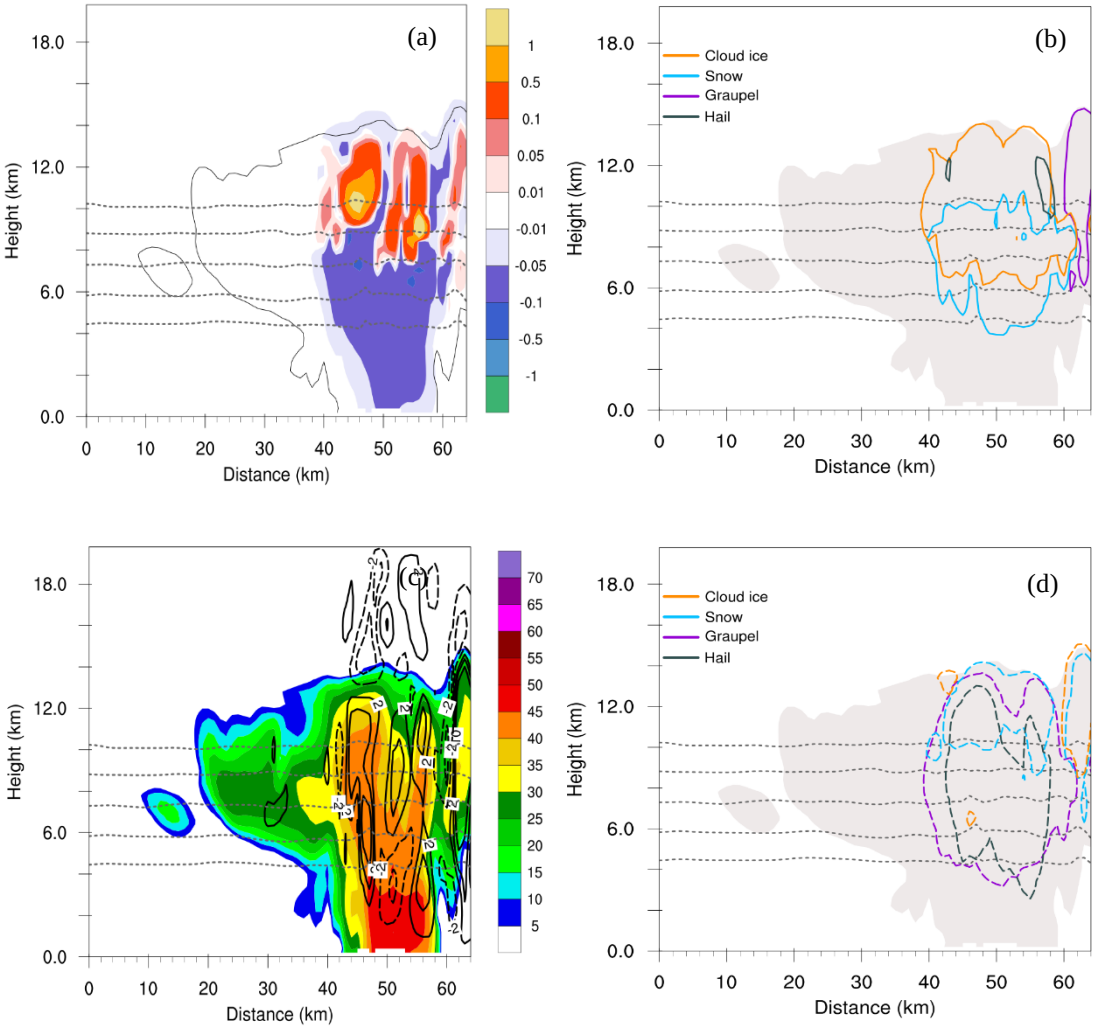

Figure R5 Vertical cross sections (south to north) at the location shown in Fig. 4f (revised version) of simulated variables during the period of maximum lightning frequency (10:36 UTC) in the P-case. (a) Total net space charge (nC m^{-3}, shaded). The 0 ℃, -10 ℃, -20 ℃, -30 ℃ and -40 ℃ isotherms are shown by dashed gray lines in (a)-(d). (b) +0.1 nC m^{-3} space charge density contours for cloud ice (orange), snow (blue), graupel (purple), and hail (black). The cloud outline (reflectivity echoes ≥ 5 dBZ) is denoted by the gray shaded contour. (c) Radar reflectivity (unit: dBZ), black lines for vertical velocities (solid line: 2, 5, 10 m s^{-1}; dashed line: -2 m s^{-1}). (d) As in (b), but for -0.1 nC m^{-3} charge density.

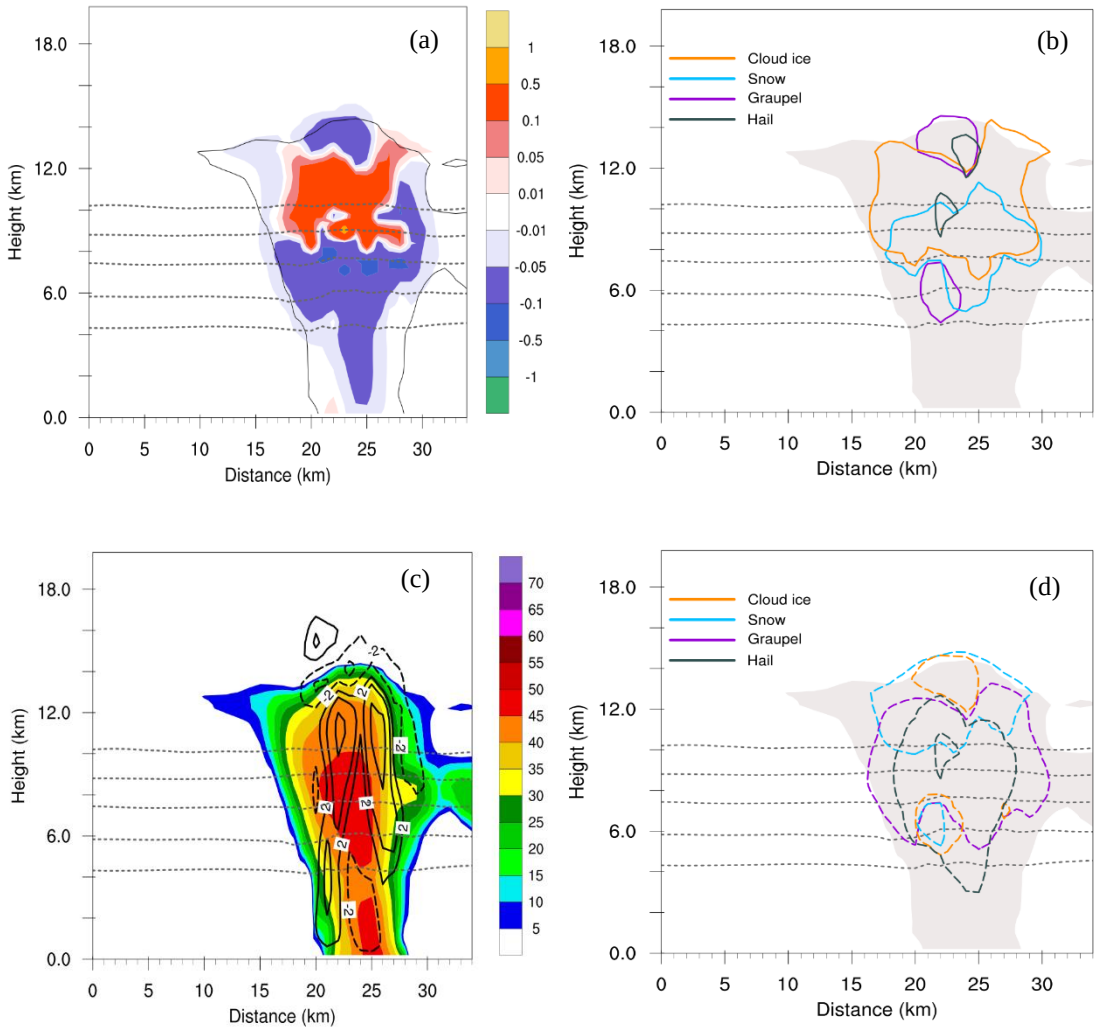

Figure R6 As in Fig. R5, but the vertical cross sections at the location shown in Fig. 4c (revised version) of simulated variables during the period of maximum lightning frequency (10:06 UTC) in the C-case.

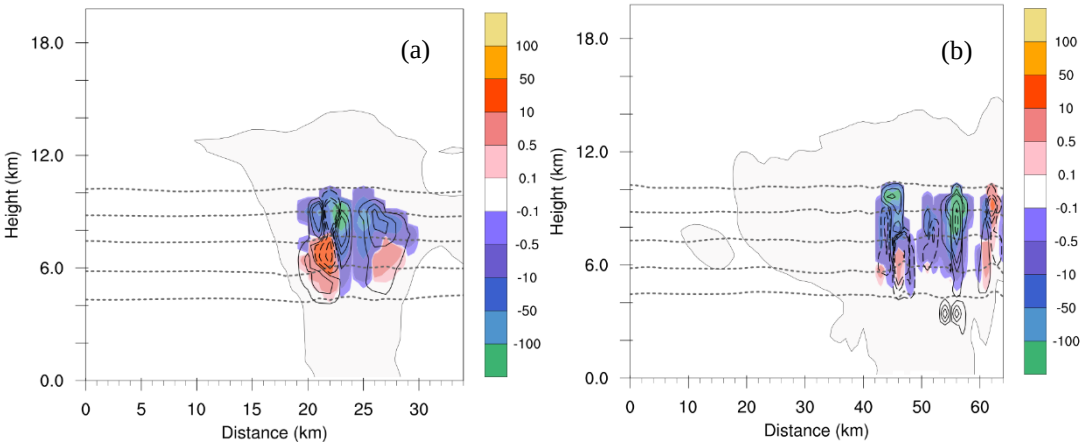

Figure R7 Vertical cross sections (south to north) at the locations shown in Fig. 4c and 4f (revised version) of non-inductive (pC m^{-3} s^{-1}, shaded) and inductive (solid lines: 0.1, 0.5, 1 pC m^{-3} s^{-1}; dashed lines: -0.1, -0.5, -1, -5, -10 pC m^{-3} s^{-1}) charging rates during the period of maximum

lightning frequency (a) C-case (10:06 UTC, Fig. 4c), and (b) P-case (10:36 UTC, Fig. 4f). The 0 ℃, -10 ℃, -20 ℃, -30 ℃ and -40 ℃ isotherms are shown by dashed gray lines.

Technical corrections:

1. Denote in Fig. 2 the regions for which the results are analyzed

2. The isotherms shown in the figures are very pale and difficult to see. It is also useful to show -30 ℃ and -40 ℃ isotherms.

3. The labels indicating the vertical velocities in Fig. 5 i and Fig.5j are blurred – they should be brighter.

4. It is better to use one and the same color for the results of C- and P-case simulation. So, it is desirable to use in Fig.4 (similar as in Fig.3b and in Fig.6) blue color for the C-case and red for the P-case.

5. The caption of Fig. 7 and others similar has to be revised because the figure does not show any microphysical characteristics.

Response:

Thanks a lot for these suggestions. All suggestions are helpful for us to improve our manuscript. We have modified in the revised version accordingly.

References:

Bruning E C, Rust W D, Schuur T J, et al. Electrical and polarimetric radar observations of a multicell storm in TELEX[J]. Monthly weather review, 2007, 135(7): 2525-2544.

Klemp J B, Wilhelmson R B. Simulations of right-and left-moving storms produced through storm splitting[J]. Journal of Atmospheric Sciences, 1978, 35(6): 1097-1110.

Kumjian M R, Ryzhkov A V, Melnikov V M, et al. Rapid-scan super-resolution observations of a cyclic supercell with a dual-polarization WSR-88D[J]. Monthly weather review, 2010, 138(10): 3762-3786.

Liu D, Sun M, Su D, et al. A five-year climatological lightning characteristics of linear mesoscale convective systems over North China[J]. Atmospheric Research, 2021, 256: 105580.

Saunders C P R, Peck S L. Laboratory studies of the influence of the rime accretion rate on charge transfer during crystal/graupel collisions[J]. Journal of Geophysical Research: Atmospheres, 1998, 103(D12): 13949-13956.

Van Den Broeke M S, Straka J M, Rasmussen E N. Polarimetric radar observations at low levels during tornado life cycles in a small sample of classic southern plains supercells[J]. Journal of applied meteorology and climatology, 2008, 47(4): 1232-1247.

Zrnic D S, Balakrishnan N, Ziegler C L, et al. Polarimetric signatures in the stratiform region of a mesoscale convective system[J]. Journal of Applied Meteorology and Climatology, 1993, 32(4): 678-693.

Interactive comment on "Aerosol Effects on Electrification and Lightning Discharges in a Multicell Thunderstorm Simulated by the WRF-ELEC Model" by Mengyu Sun et al.

M. Sun et al.

sunmengyu16@mails.ucas.edu.cn

Reply to Referee 3

The authors present a concise study of aerosol (acting as CCN) impacts on electrification and lightning activity in a case study simulation of severe deep convection over Beijing. Regional simulations are performed using the WRF model with a lightning parameterization. Two simulations are performed: a 'polluted' (P) case with CCN concentrations consistent with those observed in the Beijing area, and a 'continental' (C) case with CCN concentrations that represent standard continental conditions (but which still remain high compared to e.g. clean oceanic conditions). The model reproduces the convective event relatively well, with convection occurring slightly earlier in the model than observed. When adjusted for timing of convection, the polluted case has a similar flash count and evolution of the flash count variability to observations while the continental case has a completely different intensity and evolution of lightning flashes, with the onset of lightning occurring earlier than the polluted case but the lightning intensity being much weaker throughout the duration of convection. The authors assess the differences in the lightning activity between the two cases in terms of the cloud microphysics and show that the polluted case has increased amounts of cloud water, suppressed amounts of graupel and increased amounts of cloud ice compared to the continental case and that there are stronger updrafts and downdrafts in the polluted case. The differences in the cloud charge structure are then related to these morphological differences in the cloud microphysical structure, which is used to explain the differences in lightning evolution and intensity between the two cases. The paper is mostly well structured with informative and clear figures, however much of the discussion of the aerosol impacts on microphysical development and processes is

speculative rather than supported by thorough analysis. This is a major weakness of the study which should be addressed in a revised version of the paper before it is suitable for publication.

Response:

Many thanks for the instructive and constructive comments. We have studied them carefully and have addressed them in the revised manuscript. Below are the point-to-point responses to the reviewer's comments.

General comments:

1. The manuscript is in need of careful English language editing throughout, particularly in the abstract and introduction. There are too many for a reviewer to spend time providing a full list of typos and language corrections.

Response:

Thanks for this comment. We will improve our text following the general and specific comments below.

2. The paper would benefit from an explanation of inductive vs non-inductive charging mechanisms for the reader familiar with cloud microphysics but not charging mechanisms and lightning. Similarly, discussion of the dipole/tripole charge structure needs more explanation and placing in context of which is more likely to have occurred in the observed case.

Response:

Thanks for this comment. We have optimized the explanation of inductive and non-inductive charging mechanism, and dipole/tripole charge structure in the revised version at several parts. For example, lines 166-168, lines 170-172, lines 406-414.

Lines 167-169: "**Non-inductive (i.e., independent of external electric fields) charge separation resulting from rebounding collisions between various ice-phase particles (ice, graupel, snow, hail)**".

Lines 171-173: "**Inductive charging requires a pre-existing electric field to induce charge on the surfaces of the colliding particles (Mansell et al., 2005)**".

Lines 408-413: "**normal dipole (upper charge positive, lower charge negative; e.g., Thomas et al., 2001) …normal tripole (a dominant region of negative charge with positive charge above and a positive charge below with approximately the same order of magnitude of charge, Simpson and Scrase, 1937; William et al., 1989)**".

3. The authors make many statements about microphysical process differences between the two cases, but do not provide any analysis of these processes or comparison to what would be expected to have occurred in the real observed case.

Response:

Thanks for this comment. We have made comparison of the radar reflectivity as a function of time, hourly peak rainfall rate, and the spatial distribution of precipitation between the observation and both simulations. The comparisons show that the simulated distributions and spatio-temporal development of radar reflectivity and precipitation under polluted condition are in overall agreement with observations. In additional, we added related analysis in several part, for example: lines 251-254; lines 259-277; Figure 5, 6, and 7.

4. The authors state that certain sections of the model domain are excluded from the analysis, but then show many figures in which the microphysical structure of the two simulations are averaged horizontally. Details of this horizontal averaging process need to be given to ensure that they are consistent across all the analysis and appropriate for the particular scientific questions being addressed.

Response:

Thanks for this comment. We have defined "domain" as "**the impacts of aerosol on lightning activity will only be evaluated in the southeastern Beijing area (39.4 ℃N-40.6 ℃N, 116.0 ℃E-117.5 ℃E, shown in Fig. 4d; here on, 'domain' for short)**" (revised version, lines 256-258) and denoted in the Figure 4d (revised version). And we clarified the details of horizontal average process as follows: "**For each quantity, the mass mixing ratio and number concentration of hydrometeors are averaged over the analyzed region (denoted in Figure 2d) at a given altitude.**"(Revised version, lines 312-314)

Specific comments:

Section 3 (Model overview): the model setup up and boundary forcing should be described (with appropriate references) in the body of the text as well as summarized in a table. More information on the model setup is required: what is the simulation start time, how much spin-up time is discarded from the analysis (if at all), are both nests run without a convection scheme (I believe this is the case?), how do the authors downscale from 1-degree global data to their 6 km nest, what is the geographical coverage of the two model nests and the placement of the 2km nest inside the 6 km nest (a map would help)?

Response:

Thanks for these questions. This comment includes three questions. We will deal with these one by one.

(A) Regard the model setup.

We have added information on the model setup in the revised version (lines 207-220). And yes, both nests run without a convection scheme.

(B) Regarding how to perform nesting technique, the WRF Preprocessing System (WPS, shown in Figure R1) is used to configure real-data simulations. First, we use "geogrid" program to define dimensions and horizontal resolution of domains (here we

set the 6 km and 2 km nests). “Geogrid” also provides values for static fields at each model grid point. And then, the “ungrib” program is deployed to read GRIB files (a WMO standard file format for storing regularly-distributed fileds) and extract meteorological fields (Vtables are used to extract fields). Finally, we use the “metgrid” program to interpolate meteorological data (extracted by ungrib) to simulation domains (defined by geogrid) horizontally. More details could be found at: https://www2.mmm.ucar.edu/wrf/users/.

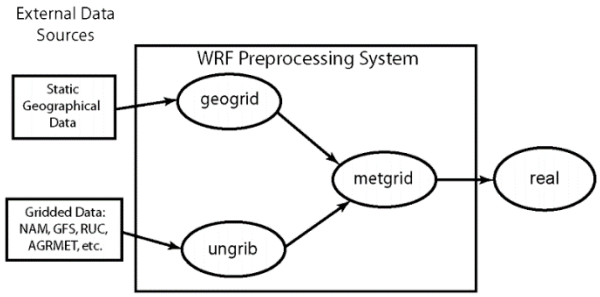

Figure R1 WPS program flowchart

(C) Regarding the geographical coverage of the two model nests

Figure R2 shows the grid domains used in all of the simulations. Since the nested domain setup has been added in the revised version (lines 207-210), we have not put in the revised manuscript.

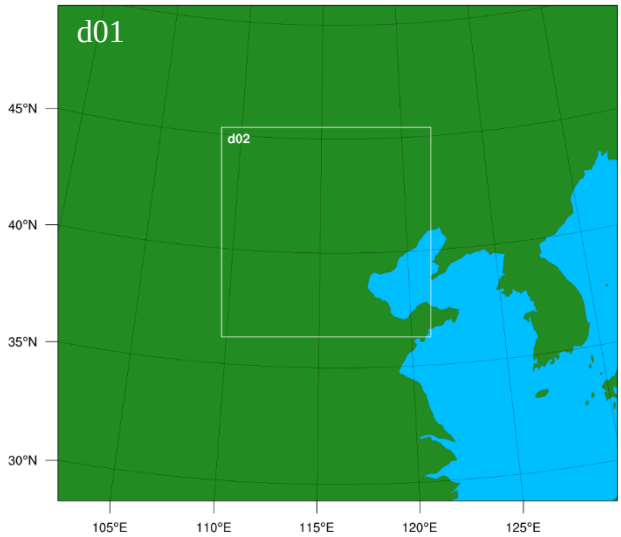

Figure R2 Grid domain used in the simulations

L154: “grids for short” - grids usually refers to the entire set of model grids (nested),

not points. I suggest using ‘points’, or just ‘grid points’.

Response:

Thanks for the suggestion. We have changed to “grid points” in the revised version.

L171: “The average value of the observed aerosol concentration before thunderstorm initiation is much higher in the Beijing area” - higher than what? And how does this compare to the two CCN concentrations you have selected as your polluted and continental values?

Response:

Thanks for this question. The hourly average mass concentration of $PM_{2.5}$ on 11 August 2017, and related references have been added in the revised version to clarify. “**The average value of the observed $PM_{2.5}$ concentration before the thunderstorm initiation (more than 110 μg m^{-3}) is much higher than the 3-year mean $PM_{2.5}$ concentration (69.4±54.8 μg m^{-3}) in the Beijing area (Liu et al., 2018).**” And the CCN concentration is selected as the polluted case which is consistent with observation. The initial number concentration for the C-case is consistent with typical continental conditions (e.g. Hobbs and Rangno, 1985; Mansell et al., 2005; Mansell, personal communication, 2019). (Revised version, lines 224-233, Figure 3)

L200-215 (and Fig 4): Does light/heavy/moderate etc refer to lightning density (flashes occurring in terms of number of grid points)? Clarify this in the wording.

Response:

Thanks for this suggestion. Yes, these four lightning intensity categories have been clarified in the revised manuscript. (Lines 291-294, Figure 9)

L233: Is the horizontal averaging performed over the entire model domain or excluding

the region in the NW where the convection was different from the observed case?

Response:

Thanks for this suggestion. We have defined "domain" as "**the impacts of aerosol on lightning activity will only be evaluated in the southeastern Beijing area (39.4 ℃N-40.6 ℃N, 116.0 ℃E-117.5 ℃E, shown in Fig. 4d; here on, 'domain' for short)**" (revised version, lines 256-258) and denoted in the Figure 4d (revised version).

Fig 5: The polluted case has an extra cell (at approx. 09:45 UTC) that doesn't develop in the continental case. Can you explain why this is and what impact this has on the results? Given that you are forcing both simulations with the same boundary data, this may affect the subsequent development of convection in the P-case compared to the C-case.

Response:

We appreciate this suggestion. In light of this comment, we have analyzed the radar reflectivity and precipitation (Figure 6, 7, revised version) at the beginning stage of the thunderstorm for the observation and both simulations. Since the observed radar reflectivity during 11:00-11:24 UTC is missing, so Figure R3 shows the radar echo before and after 11:15 UTC (09:45 UTC in simulations) for comparison. In the early stage of the thunderstorm, the radar echo for the P-case is relatively similar with these of the C-case. We realized that the area we chose in the initial stage was too small. The extra cell in figure 5j (initial version) probably because that the previous selected area did not include the cell in the C-case. Therefore, we have enlarged the region (shown in Figure 4d, revised version). The microphysics along with further electrification and lightning activities of this thunderstorm have been re-analyzed. The dynamic-thermodynamic processes do affect the development of thunderstorm significantly (e.g. Williams et al., 2005; Guo et al., 2016; Wang et al., 2018; Zhao et al., 2020), the re-analyzed results still suggest that under polluted condition lightning activity is

significantly enhanced. Moreover, the precipitation duration is longer under polluted condition (Figure 10c and 10d, revised version), which also provides evidence for the enhancement of convection. With such improvements, we believe the analysis of the physical processes is much appropriate for explaining the difference in the electrification and discharging in both simulated cases.

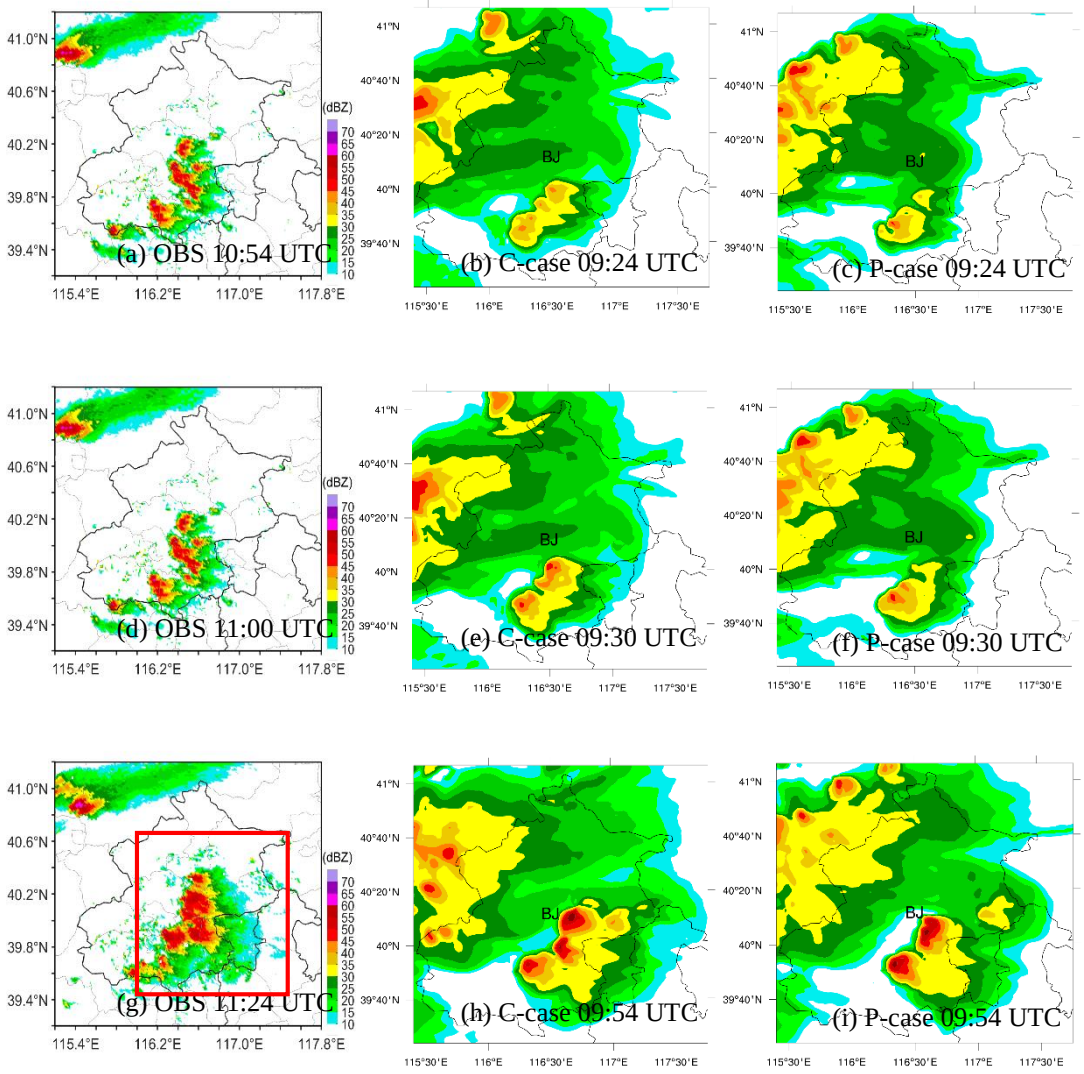

Figure R3 Radar reflectivity (unit: dBZ) between observation and simulation for the C- and P-cases, the simulation was earlier than observation about 1.5 h. (a), (d), (g) Observation at 10:54 UTC, 11:00 UTC and 11:24 UTC. (b), (e), (h) Simulation for the C-case at 09:24 UTC, 09:30 UTC and 09:54 UTC. (c), (f), (i) Simulation for the P-case at 09:24 UTC, 09:30 UTC and 09:54 UTC, respectively. The red rectangle in Fig. R3g denotes the region where the simulated results are analyzed in this study.

L336: “microphysical and electrical processes” - do the authors mean the CCN have a direct electrical impact on the charging, and not just through the impact on microphysics?

Response:

Thanks for this question. This sentence has been modified as follows: “**indicating that aerosol plays an important role in affecting the accumulated charge density through microphysical and further electrical processes**”. (Revised version, lines 447-448)

L350: discussion on convective strength - at the start of this section you say there is no significant difference in convective strength between the two cases, but it was stated in L320 that the P-case has stronger updrafts and downdrafts than the C-case. This contradicts saying “vertical convective strength did not vary significantly under different aerosol conditions”. Similarly at the end of this section you then say there is increased latent heating at upper levels that strengthens convection and enhances lightning activity (L364), which contradicts the first sentence which says there is no difference in convective strength.

Response:

These are good questions and comments. For clarity, we have used the temporal variation of the vertical profiles of peak latent heating (Figure 12, revised version) to make comparison of latent heat between both simulations during the whole duration of the thunderstorm. The latent heat shown in Figure 12 results from both condensation and freezing. For the condensation latent heat, we modified the related analysis in Part “**4.2 Microphysical properties of multicell”,** for example:

Lines 323-329: “**Under polluted condition, more aerosols could be activated into cloud droplets and more water vapor condenses onto these droplets, leading**

to large cloud water content and small droplet size (Lynn et al., 2007; Wang et al., 2011; Zhao et al., 2015; Jiang et al., 2017). Thereby, relatively more latent heat of condensation released in the P-case where large cloud water content exists, which can be seen in the vertical distribution of peak latent heat (Figure 12)."

For the frozen latent heat, the related analysis has been added as follows: "**the maximum of peak latent heat in the P-case occurs above 10 km at 09:30 UTC (Figure 12), indicating that more cloud droplets are lifted to the upper levels (< -40 ℃) and converted into ice crystals at the beginning stage of the thunderstorm. … The high value of latent heat existed in the higher levels (above 10 km) reveals a large amount release of frozen latent heat. Previous studies also found that elevated aerosol loading contributed to the increasing frozen latent heat (e.g., Khain et al., 2005; Lynn et al. 2007; Storer et al., 2010; Li et al., 2017).**"(Revised version, lines 349-356)

L445: The authors note here that their study only considers aerosol impacts on this case of convection through perturbations to the liquid phase development of the cloud. One question might then be what are the dominant aerosol sources observed in the case study region, particularly at the time of this event, and whether they are more effective CCN or IN?

Response:

Thanks for this question. As for the aerosol sources, we analyzed the concentration of SO_4^{2-}, NO_3^-, Cl^-, NH_4^+ in the case, which could be treated as effective source of CCN. Black carbon (BC) and organic matter (OM), which are believed to be effective IN (Murray et al., 2010), are also taken into consideration. As shown in Figure R4, the mass fraction of BC in $PM_{2.5}$ is rather small (< 3%), which is consistent with Liu et al. (2020). According to Zhang et al. (2013), soil dust, organic carbon (OC), and BC had similar patterns of waning in the summer. Based on these analysis, we only consider

aerosol impacts on lightning acting as CCN. In this case, the proportion of OM in PM_1 is little higher than that of NH_4^+ and SO_4^{2-}. The effect of IN on the microphysical and electrical processes will be considered in our future study.

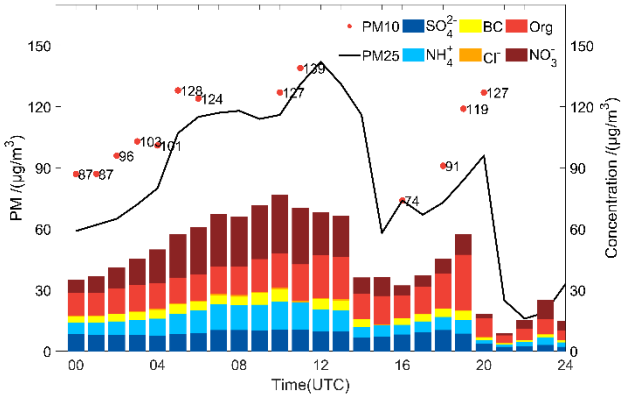

Figure R4 Hourly mass concentration of $PM_{2.5}$, PM_{10} and chemical composition of PM_1 [SO_4^{2-}, NH_4^+, NO_3^-, Cl^-, black carbon (BC), organic matter (Org)] at urban area. The black line represents $PM_{2.5}$, the red dots represent PM_{10}, and the columns represent different chemical composition. The real-time hourly average ground levels of $PM_{2.5}$ are from the China National Environmental Monitoring Center. Other sampling site is located on the tower campus of the State Key Laboratory of Atmospheric Boundary Layer Physics and Atmospheric Chemistry (LAPC), Institute of Atmospheric Physics (39.97 °N, 116.37 °E).

Technical corrections:

Fig 3b and Fig 6 captions: the colours should be noted as well as linestyle. In fact, it would be better to use one of either (a) colour or (b) linestyle to denote the two cases, not a combination of both.

Response:

Thanks for this suggestion. We have modified accordingly.

References

Liu H, Pan X, Liu D, et al. Mixing characteristics of refractory black carbon aerosols at an urban site in Beijing[J]. Atmospheric Chemistry and Physics, 2020, 20(9): 5771-5785.

Liu Z, Gao W, Yu Y, et al. Characteristics of PM 2.5 mass concentrations and chemical species in urban and background areas of China: emerging results from the CARE-China network[J]. Atmospheric Chemistry and Physics, 2018, 18(12): 8849-8871.

Murray B J, Wilson T W, Dobbie S, et al. Heterogeneous nucleation of ice particles on glassy aerosols under cirrus conditions[J]. Nature Geoscience, 2010, 3(4): 233-237.

Zhang R, Jing J, Tao J, et al. Chemical characterization and source apportionment of PM 2.5 in Beijing: seasonal perspective[J]. Atmospheric Chemistry and Physics, 2013, 13(14): 7053-7074.